

# Massively Parallel Probabilistic Computing with Sparse Ising Machines

Navid Anjum Aadit,<sup>1,\*</sup> Andrea Grimaldi,<sup>2</sup> Mario Carpentieri,<sup>3</sup> Luke Theogarajan,<sup>1</sup>  
John M. Martinis,<sup>4,5,6</sup> Giovanni Finocchio,<sup>2,†</sup> and Kerem Y. Camsari<sup>1,‡</sup>

<sup>1</sup>*Department of Electrical and Computer Engineering,*

*University of California, Santa Barbara, Santa Barbara, CA, 93106, USA*

<sup>2</sup>*Department of Mathematical and Computer Sciences, Physical Sciences and Earth Sciences,*  
*University of Messina, Messina, Italy*

<sup>3</sup>*Department of Electrical and Information Engineering, Politecnico di Bari, Bari, Italy*

<sup>4</sup>*Department of Physics, University of California, Santa Barbara, Santa Barbara, CA, 93106, USA*

<sup>5</sup>*Quantala, Santa Barbara, CA, 93105, CA, USA*

<sup>6</sup>*Zyphra Technologies Inc., San Francisco, CA, USA*

(Dated: October 7, 2021)

Inspired by the developments in quantum computing, building quantum-inspired classical hardware to solve computationally hard problems has been receiving increasing attention. By introducing systematic sparsification techniques, we propose and demonstrate a massively parallel architecture, termed sIM or the sparse Ising Machine. Exploiting the sparsity of the resultant problem graphs, the sIM achieves ideal parallelism: the key figure of merit — flips per second — scales linearly with the total number of probabilistic bits (p-bit) in the system. This makes sIM up to 6 orders of magnitude faster than a CPU implementing standard Gibbs sampling. When compared to optimized implementations in TPUs and GPUs, the sIM delivers up to  $\approx 5 - 18\times$  measured speedup. In benchmark combinatorial optimization problems such as integer factorization, the sIM can reliably factor semi-primes up to 32-bits, far larger than previous attempts from D-Wave and other probabilistic solvers. Strikingly, the sIM beats competition-winning SAT solvers (by up to  $\approx 4 - 700\times$  in runtime to reach 95% accuracy) in solving hard instances of the 3SAT problem. A surprising observation is that even when the asynchronous sampling is made inexact with simultaneous updates using faster clocks, sIM can find the correct ground state with further speedup. The problem encoding and sparsification techniques we introduce can be readily applied to other Ising Machines (classical and quantum) and the asynchronous architecture we present can be used for scaling the demonstrated 5,000–10,000 p-bits to 1,000,000 or more through CMOS or emerging nanodevices.

## I. INTRODUCTION

Markov Chain Monte Carlo (MCMC) algorithms have made a significant impact in the history of computing [1]. MCMC methods are among the most powerful randomized algorithms with a wide range of applications in Artificial Intelligence (AI) [2]. Powerful MCMC methods such as Metropolis and Gibbs sampling have been widely applied to training generative neural networks [3], probabilistic inference in belief networks [4], calculating physical observables in classical and quantum systems [5, 6] and solving computationally hard combinatorial optimization problems [7].

Designing domain-specific hardware to accelerate such computationally hard problems of AI has been receiving increasing attention with the slowing pace of Moore’s Law. There have been a number of approaches to build special-purpose hardware to solve computationally hard problems. A class of such solvers (also known as Ising Machines) specifically solve quadratic energy models or the Ising model, typically mapped to problems in NP [8–25],

$$E = - \left( \sum J_{ij} m_i m_j + \sum h_i m_i \right) \quad (1)$$

( $m_i \in \pm 1$ ,  $J_{ij}, h_i \in \mathbb{R}$ ), where quadratic terms ( $m_i m_j$ ) in the energy translate to a linear “synapse” or an interconnection

matrix which can be expressed as a graph ( $I_i = -\partial E / \partial m_i$ ):

$$I_i = \sum J_{ij} m_j + h_i \quad (2)$$

Choosing the activation function of individual probabilistic bits as

$$m_i = \text{sgn} [\tanh(\beta I_i) - \text{rand}_U(-1, 1)] \quad (3)$$

ensures the system states,  $\{m\}$ , are visited according to their corresponding Boltzmann probability:

$$p_i \propto \exp [-\beta E(\{m\})] \quad (4)$$

where  $\beta$  is introduced as an “inverse temperature” and can be used to enhance or suppress probabilities corresponding to energy minima. The dynamical evolution of Eq. (2)-(3) enables probabilistic sampling and inference, learning weights of a stochastic neural network or performing search or optimization in the exponential state space of the model. Such a machine evolving to the Boltzmann distribution defined by Eq. (4) is called a Boltzmann Machine, after the pioneering work of Hinton and colleagues [26, 27].

So far, nearly all dedicated Ising Machines have specifically focused on optimization problems, with the exception of D-Wave’s quantum annealers which have been applied to problems beyond combinatorial optimization [28, 29].

Typically in Gibbs sampling (a type of MCMC method), Eq. (2)-(3) are updated iteratively to dynamically evolve the Markov chain such that the network eventually reaches the

\* [maadit@ece.ucsb.edu](mailto:maadit@ece.ucsb.edu)

† [giovanni.finocchio@unime.it](mailto:giovanni.finocchio@unime.it)

‡ [camsari@ece.ucsb.edu](mailto:camsari@ece.ucsb.edu)

Boltzmann distribution defined by Eq. (4). A practical difficulty lies in the serial nature of this evolution: connected nodes need to be updated one after the other since parallel updating leads to repeated oscillations in the network state, preventing the network from converging to the Boltzmann distribution. The need for sequential updating inherently serializes the network evolution, signified by the nested for-loops in standard descriptions of Gibbs sampling [30].

## II. SUMMARY OF MAIN RESULTS

This paper is about overcoming the fundamental difficulty of sequential updating by combining algorithmic and architectural ideas to build a sparse Ising Machine (sIM) for solving combinatorial optimization and probabilistic sampling problems. The sIM in this paper is based on a Field Programmable Gate Array (FPGA) implementation however the architecture is general and it can have different implementations. The sIM achieves near-ideal parallelism for MCMC sampling as long as the interconnection matrix  $J$  is sparse. A key feature of our framework is in its generality: we first show that *any* optimization function can be efficiently represented as a sparse (but irregular) graph through principles of invertible logic [22, 31]. We then outline techniques for further sparsification using additional nodes without any approximation. Next, we develop a massively parallel architecture to implement Eq. (2)-(3), exploiting the sparsity of the graph, where the graph is defined by  $J$ . This is achieved by using multiple phase shifted clocks controlling the activation of probabilistic bits (p-bits) (Eq. (3)). The p-bits are interconnected through a multiply-accumulate (MAC) unit (Eq. (2)) (see Supplementary Fig. S2c for the architecture). This architecture can be considered to be a low level hardware-level implementation of chromatic Gibbs sampling [32] where large blocks of conditionally independent nodes are updated in parallel. For this sampling to be exact, the MAC must finish its computation before the next color block is updated. An unexpected finding however is even when color blocks are updated before the MAC operation is completed, the network is often able to find exact ground states in model optimization problems. This inexact Gibbs sampling approach is reminiscent of the Hogwild!-Gibbs algorithm [33] and we show how this over-clocking idea can lead to further advantages.

The idea of block updating is commonly used for regular graphs. For example, as first noted in Ref. [34], when the graph is bipartite (as in Restricted Boltzmann Machines or chessboard lattices), a trivial coloring (with two colors, black and white) is possible and this is often exploited in updating each color block in parallel [4, 19, 35–37]. We also note that parallelization techniques in multiple FPGAs have recently been explored for other types of Ising Machines [24], however these are based on completely different algorithms unrelated to the computational model we use based on Eq. (2)-(4).

In this paper, we extend the block updating scheme so that it applies to regular *and* irregular graphs with the only requirement that the graphs are sparse enough to be colored by as few colors as possible. We find that when the overall graph

density is low (e.g.,  $\lesssim 1\%$ ), irregular graphs containing nodes with hundreds of neighbors can be colored by a few colors in line with theoretical results on coloring sparse graphs [38]. Further, we provide sparsification methods to limit the maximum neighbors of given graphs, without introducing approximations.

We tested the resultant sIM on model problems and achieved three key results:

- In solving Boolean satisfiability problems, the sIM is able to beat competition-winning SAT solvers (2020, 2017) in run-time by up to 4-700x to reach 95% accuracy.
- In probabilistic sampling, the sIM delivers a measured 5-18x speedup over the optimized TPU and GPU implementations (Table I). Against a standard CPU implementation, we measure up to 6-orders of magnitude speedup.
- In integer factorization, the sIM can reliably find the absolute ground state for semiprimes up to 32-bits, far larger than what has been reported for D-Wave’s quantum annealers or similar probabilistic solvers [15, 20, 22, 39–41] (Table II). Robust factorization up to 32-bit numbers seem to be the largest by far among these alternatives.

In this paper, we use integer factorization as a computationally hard optimization problem to compare the performance of sIM with respect to D-Wave and other Ising Machines. Expressing the integer factorization problem as a satisfiability (or spin-glass) instance is not expected to be practically relevant, as studied in detail in Ref. [42]. However, critical subroutines of the best algorithms for factoring may potentially be accelerated using improved satisfiability through dedicated hardware or algorithms [43].

A striking result is to show speedups over recent competition-winning SAT solvers in approximate optimization, since SAT solvers have been optimized and fine-tuned after decades of research and development. In contrast, the sIM is using a standard simulated annealing algorithm without any detailed fine-tuning. Further improvements using more sophisticated algorithms such as Parallel Tempering should increase the performance of the sIM. Moreover, experimental developments in emerging nanodevice technologies [44, 45] such as Magnetic Tunnel Junction based asynchronous probabilistic computers [15] can use the same architectural and algorithmic ideas we develop in this paper to provide additional speedup [25].

The organization of this paper is as follows: Section III shows how any combinatorial optimization problem can be converted to an invertible probabilistic circuit (p-circuit) using the basic building blocks (AND, OR, NOT, Full Adder) with compact interconnection matrices and discrete weights. We illustrate in Section IV how a given sparse p-circuit can be colored with a few colors using an approximate graph coloring algorithm, DSATUR [46]. We elaborate on the details of the hardware architecture implementing the coupled equations and propose further sparsification techniques to overcome the

limitations of high fan-out circuits. Next, we report our experimental results on the problem of integer factorization and the Boolean satisfiability problem in Sections V-VII as well as detailed comparisons of the sIM with respect to CPU, GPU and TPU implementations of MCMC.

### III. COMPOSING INVERTIBLE LOGIC CIRCUITS FROM ELEMENTARY GATES

Invertible logic (discussed in detail in Refs. [31, 47]) allows composing probabilistic generalizations of a universal set of basic gates such as COPY/NOT (2 p-bits), AND (3 p-bits), OR (3 p-bits) and Full Adders (FA, 5 p-bits). The basics of such invertible gates and their operation have been discussed extensively [22, 48, 49]. Here, we show some of the  $J$  matrices for a set of elementary probabilistic gates in the Supplementary Information, Section I, where we also elaborate on how to compose p-circuits corresponding to any given Boolean function. Similar to conventional digital circuits, the use of basic p-logic gates to a hierarchical design of larger p-circuits results in highly sparse representations amenable to the massive parallelism discussed in this paper.

The ability of invertible logic circuits to operate in reverse gives rise to a convenient method of solving inverse problems, as noted in the related paradigm of memcomputing and by D-Wave [39, 50]. Therefore, hard combinatorial optimization problems such as integer factorization and Boolean satisfiability (SAT) can be solved in hardware using invertible multipliers or by invertible Boolean circuits corresponding to a given satisfiability instance. Fig. 1a shows a classic  $m$ -bit multiplier circuit composed of multiple AND gates and FAs. In the reverse direction, this circuit works as an  $n$ -bit factorizer circuit ( $n = 2m$ ) where we clamp the output bits to the  $n$ -bit product to be factored. Similarly, we clamp the output of the SAT solver circuit in Fig. 1b to 1 and find the input variables satisfying all the clauses in the reverse direction. Each clause is represented by multiple OR gates; if any input variable is negated, we modify the corresponding weight ( $J$ ) matrix of the OR gate accordingly. The output bits of the OR gates can be clamped to 1 either directly or by using an AND gate at the end. In this work, we primarily focus on the 3SAT, a special form of the satisfiability problem where each clause has exactly three variables in the conjunctive normal form (CNF) [51]. We collected 3SAT instances as ‘.CNF’ files from the UBC SATLIB library [52] and map them to interconnection matrices ( $J$ ), composed of elementary probabilistic gates.

### IV. GRAPH COLORING FOR MASSIVE PARALLELIZATION

When a quadratic energy model described by Eq. (1) is chosen, an invertible logic p-circuit can be represented as a graph where each node represents a p-bit and each edge represents the connection between the p-bits. Fig. 1c illustrates the graph of an 8-bit factorizer p-circuit encoded with 52 p-bits.

As discussed in Section I, the coloring is used to exploit

the trick that allows the parallel update of unconnected (conditionally independent) p-bits. We first color the graph using a heuristic graph coloring algorithm DSATUR [46]. Coloring a graph with exactly the minimum number of colors is NP-hard [53]. However, this is unimportant for our purposes since we use DSATUR as an efficient (polynomial) coloring algorithm, which may or may not find the optimum coloring. We find that as long as the starting graph is sparse only a few colors are needed for the invertible logic problems we have considered. For example, for the 8-bit factorizer graph only five colors are used and as a result, we need five parallel and equally phase-shifted clocks in the sIM (Fig. 1d). The equal phase shift is required to avoid any concurrent edges of the clocks. In our architecture (Supplementary Information, Fig. S2b,c), different color blocks receive different clocks to their RNGs, ensuring no two connected p-bits flip at the same time for exact Gibbs sampling. This is a constraint we relax in Section V.

In the case of exact Gibbs sampling, our architecture ensures the entire network is updated in parallel in one clock period (of any color) while ensuring an effectively sequential operation.

As a quantitative measure of sparsity in the resultant invertible p-circuits we use the notion of graph density  $\rho$ . For an undirected graph  $\rho$  is defined as

$$\rho = \frac{m}{\frac{1}{2}n(n-1)} \quad (5)$$

where  $n$  is the number of nodes, corresponding to the number of p-bits in the sIM and  $m$  is the number of edges, corresponding to the interconnections in the  $[J]$  matrix. With this definition an all-to-all (or a complete) graph has a  $\rho$  of 100%. We find that when p-circuits are composed of universal gates, both the factorization and the satisfiability graphs are sparse. For example, consider the graph of a 32-bit factorizer p-circuit presented in Fig. 1e having 784 p-bits with a  $\rho$  of 1.03%, requiring only 5 distinct colors. In this example, five parallel and equally phase-shifted clocks in the sIM are adequate to implement this p-circuit for massively parallel computation.

However, there is a limitation on the clock speed depending on the maximum number of neighbors for each p-bit. The neighbor distribution of the 32-bit factorizer graph reveals that it has 32 p-bits with 32 neighbors (Fig. 1e). In order to ensure every single color block is updated with the latest state of each neighbor, the MAC unit implementing Eq. 2 needs to finish its computation before the next color block is updated. With binary models the multiplication consists of simple multiplexing (the weights are either selected or they are ignored). This means that the addition for the weights needs to be completed within the  $n^{\text{th}}$  of a clock period, where  $n$  is the number of colors. In the present example, this requires large adders to add 32 s-bit numbers within this short period, where  $s$  is the bit precision of the weights.

Therefore even when the sparse graphs as in Fig. 1(e)-(g) require a few colors the p-bits with 32 or 498 neighbors introduce large synapse (addition) delays creating a severe bottleneck for how fast the clocks can be operated. To overcome this limitation we develop exact sparsification techniques to remove the nodes with a large number of neighbors without



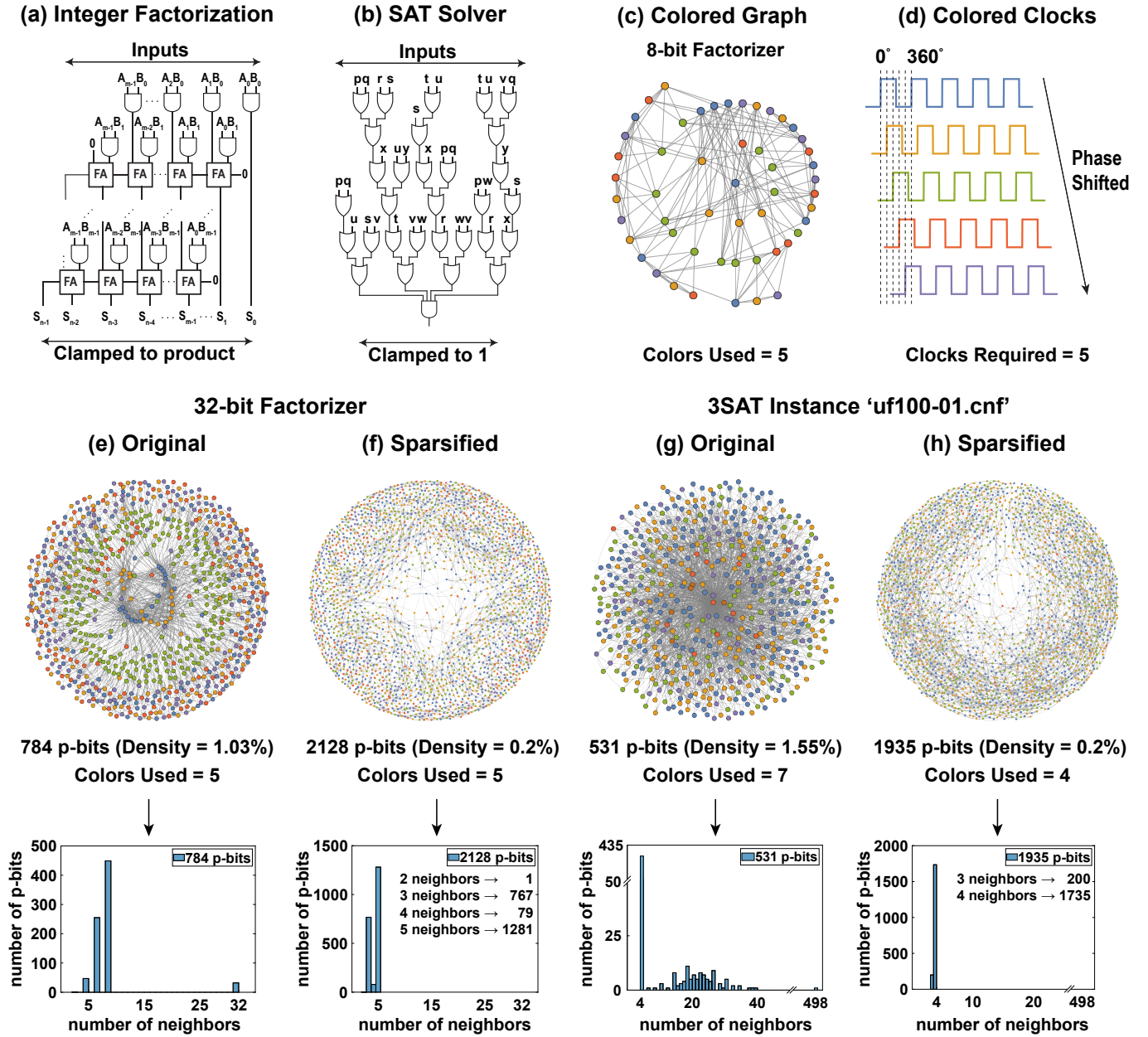


**FIG. 1.** Combinatorial optimization with invertible logic. (a) An  $n$ -bit digital multiplier composed of AND gates and full adders (FAs) that can be run invertibly to solve the integer factorization problem. (b) A Boolean circuit composed of OR and AND gates that can be run invertibly to solve satisfiability problems. (c) An example 8-bit factorizer p-circuit, illustrating how the corresponding graph can be colored with 5 colors. (d) This in turn requires 5 parallel and equally phase-shifted clocks in the sIM to implement the 8 bit-factorizer in a massively parallel architecture. (e) The original graph of a 32-bit factorizer developed using invertible logic requires 5 colors but it contains nodes with up to 32 neighbors, limiting hardware implementations. (f) Exact sparsification techniques are used to reduce nodes with a large number of neighbors at the expense of additional bits. (g) The original version of the 3SAT instance ‘uf100-01.cnf’ developed using invertible logic. (h) The sparsified version with only nodes having a maximum of 4 neighbors only. Graph density,  $\rho$  is defined by Eq. (5).

changing the structure of the optimization problem. The main idea in this approach is to split a given p-bit representation between two p-bits coupled by a ferromagnetic ( $J > 0$ ) interaction which we call a COPY gate [19, 54, 55]. The ferromagnetic interaction ensures that at the end of an annealing schedule (high  $\beta$ ), the ground states of the split and fused models are identical. We show a formal proof in the Supplementary

Information Section J.

Fig. 1f shows the sparsified graph of the 32-bit factorizer p-circuit with 2128 p-bits and a graph density of 0.2%. It is colored with 5 colors as before, however, the neighbor distribution reveals the maximum number of neighbors is limited to 5 which minimizes the adder delay and allows fast clocks. In general, such sparsification techniques always introduce extra



p-bits, however, in scaled implementations individual p-bits are almost always cheaper than complicated synapse interactions. The precise relationship between sparsification and the added number of p-bits is illustrated in Supplementary Information, Fig. S5.

Similarly, the original graph of the 3SAT instance ‘uf-100-01.cnf’ can be colored using 7 colors (Fig. 1g). It is also a sparse graph with 531 p-bits and a graph density of 1.55%. However, the neighbor distribution shows that some p-bits have more than 5 connections and one p-bit has 498 connections. This p-bit corresponds to the node where the outputs of all clauses meet. A sparsified version of this graph is illustrated in Fig. 1h with 1935 p-bits and a graph density of 0.2%. As before, the sparsification ensures the graph has a maximum of 4 neighbors for each p-bit and hence avoids large adder delays, requiring 4 colors (clocks).

In the following sections, we present our results for integer factorization and SAT solving implemented in the massively parallel sIM architecture. We implemented the sIM architecture on a Xilinx Virtex UltraScale+ FPGA VCU118 Evaluation board for our experiments. We used MATLAB device communication.

The details of the FPGA architecture and its design choices are included in the Supplementary Information, Section G. We have used a simple simulated annealing algorithm [56] for all the experiments reported in this work. We have tried different annealing schedules such as geometric, quadratic, linear, and logarithmic and found no significant difference in performance with respect to these schedules. We have used a linear schedule for simplicity for all the results we present.

## V. COMPARING SPARSE ISING MACHINE WITH EXISTING HARDWARE (CPU, GPU AND TPU)

### A. CPU comparison with approximate factoring

To compare CPU and sIM performance, we define approximate factorization as reaching 99% of the absolute ground energy from 14-bit to 50-bit semiprimes. While finding approximate factors is not useful for the problem of integer factorization, many other optimization problems benefit from high-quality and approximate solutions. As such, we treat approximate factorization as a benchmark to compare CPU and sIM performance.

We use the same annealing schedule and the same sparsified graphs for the comparison between an unoptimized MATLAB implementation on a CPU and the FPGA implementation of our sIM. For each problem, we have attempted to factor 10 different numbers 10 times to make sure we collect enough statistics and test the robustness of the system. We do not compare the performance based on exact factorization since the absolute ground state is very difficult to be reached using simulated annealing [56] and the CPU practically never reaches there.

Before we show the performance of the sIM vs CPU on solving the approximate integer factorization problem, we first focus on a key figure of merit, namely, the flips per second

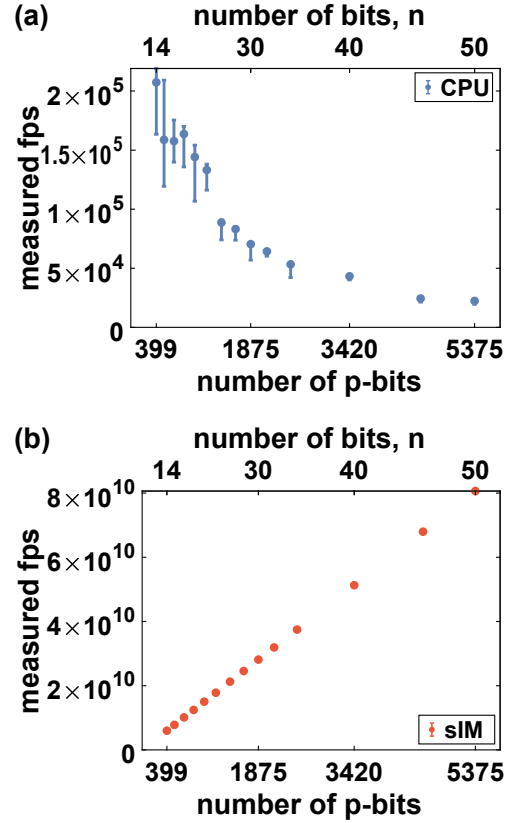


**FIG. 2.** Flips per second (fps) comparison of the sIM with a CPU. (a) The CPU fps as a function of graph size is shown, larger graph sizes drastically limiting the fps (b) The measured sIM fps as a function graph size is shown, showing ideal parallelism with increasing size. At the highest fps, the sIM delivers a  $\approx 10^6 \times$  improvement of the CPU. The error bars are obtained by taking 100 measurements of fps for each problem showing the maximum-minimum fluctuations.

(fps). The fps corresponds to the *correlated* flips per second that can be taken by the system where every flip is made based on the latest state of the network, between physically connected nodes while avoiding simultaneous updates. Indeed, various hardware implementations for MCMC solvers have reported this metric [36, 37, 57, 58]. The fps can be thought of as the effective processing speed for MCMC. The key point of the parallel architecture we design for the sIM is that its fps *increases linearly* with the number of p-bits corresponding to a problem.

Fig. 2 presents a comparison of fps between the inherently sequential CPU and the massively parallel sIM for the factorization problem. The CPU calculation is done in MATLAB by an iterative solution of Eq. (2)-(3) using standard Gibbs sampling [30] with simulated annealing. Even though optimization techniques including graph coloring by multiple threads could improve our MATLAB implementation, these should not change our conclusions since fps between the CPU and sIM differ by 6-orders of magnitude.

MATLAB runs on the Knot Cluster at the Center for Scientific Computing (CSC) server, UCSB featuring an Intel Xeon Processor E5630 running at up to 2.8 GHz. On the other hand,

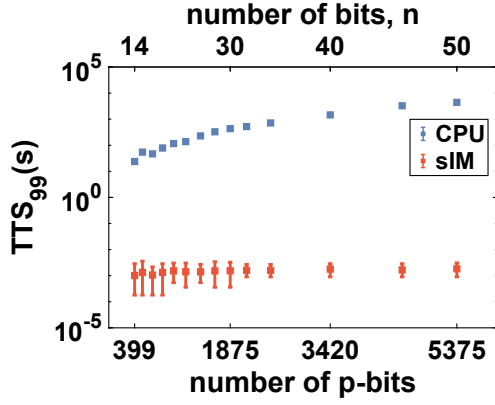


**FIG. 3.** Time to solution comparison for approximate factorization between the CPU and the sIM as a function of problem size.  $TTS_{99}$  or time to solution, is defined as the time to reach 99% of the ground state.  $TTS_{99}$  requires up to 4408.93 s for the 50-bit factorization in the CPU. For the sIM, it is showing almost a flatline behavior with up to  $\approx 10^6\times$  performance improvement. The error bars are obtained by reporting  $TTS_{99}$  to approximately factor 10 different numbers 10 times for each problem showing the maximum-minimum fluctuations.

we have used five equally phase-shifted 15 MHz clocks in the sIM and assigned those clocks to the p-bits based on a previously calculated graph coloring. In the sIM, each p-bit updates in parallel, achieving an effective clock speed of  $N \times 15$  MHz where  $N$  is the number of p-bits. 15 MHz is chosen to satisfy the timing requirements for the additions to be completed and better FPGAs or hardware implementations can be envisioned to reach even higher frequencies.

It is important to note that we directly measured the flips per second of the sIM by means of specially designed reference counters in the FPGA. The maximum flips per second (fps) achieved by the CPU is limited to around  $10^5$  (Fig. 2a). Moreover, fps quickly starts to decline for the CPU with the increasing number of p-bits. The reason for this can be attributed to the sequential nested for-loops, memory caching and large matrix multiplications. On the contrary, the sIM reaps an enormous benefit from massive parallelism, collecting up to 80 - 100 billion fps for the highest problem sizes. Crucially, the fps increases linearly with the increasing number of p-bits as shown in Fig. 2b due to its massively parallel architecture. Starting at an fps of  $5.99 \times 10^9$  for the 14-bit factorization, it achieves a maximum fps of  $8.06 \times 10^{10}$  for the 50-bit factorization. The error bars are obtained by taking 100 measurements of the fps for each problem to show the maximum and the minimum difference from the average fps. The same approach is followed for all fps reported in this work.

While we do measure an increasing fps for the sIM as a function of problem size, an important arising question is whether all these samples are useful or not. In order to test this question, we define a performance metric, the time to solution,  $TTS_{99}$  as the time to reach 99% of the absolute ground energy. Note that in the case of factorization, the exact solution is planted, in other words, we know the factors of a given product and therefore we have access to the exact ground state

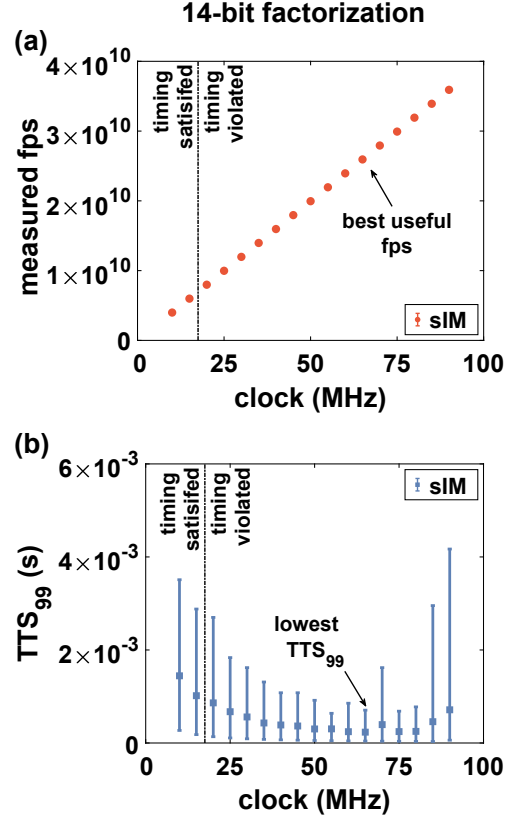


**FIG. 4.** Overclocking to improve approximate factoring. (a) For the 14-bit factorization, we measure the flips per second (fps) as a function of individual clocks feeding each color block. Timing is violated after 15 MHz. Based on (b), we observe that overclocking effectively improves fps up to 65 MHz. (b) Time to solution to reach 99% of the ground state,  $TTS_{99}$ , measured as a function of clock frequency. Despite errors in implementing Gibbs sampling, performance improves up to 65 MHz. The error bars are obtained by taking 100 measurements of fps and reporting  $TTS_{99}$  to approximately factor 10 different numbers 10 times at each clock speed showing the maximum-minimum fluctuations.

energy. Fig. 3 shows a steep rise of  $TTS_{99}$  from 14-bit to 50-bit factorization for the CPU. The fastest case requires  $TTS_{99}$  of 23.84 s for the 14-bit factorization while the slowest one requires 4408.93 s for the 50-bit factorization. In contrast, the sIM shows a roughly constant mean value for all the problems, requiring 1.02 ms for the 14-bit factorization and 1.84 ms for the 50-bit factorization (See Section IX for  $TTS$  measurement details). The 50-bit factorization is over a  $2.4 \times 10^6\times$  improvement over the CPU. The difficulty of the approximate factorization is clearly increasing with increasing problem size. The reason for the constant time to solution for the sIM despite the increasing difficulty of the problem for larger problem sizes can be attributed to the massive parallelism of the sIM where increasing problem size also increases the fps. Therefore, we can conclude that the measured fps shown in FIG. 2 is a real improvement. This makes the massive parallelism of the sIM very different from trivially parallel p-bits sampling independently.

## B. Overclocking to improve approximate factoring

The results we present in FIG. 2-3 correspond to the *exact* Gibbs sampling taken according to Eq. (2)-(3). The massively parallel architecture we present updates p-bits in parallel while ensuring every single update is made with the latest network state, as required by Gibbs sampling. In the present examples, the exact Gibbs sampling requirement resulted in 15 MHz clocks, dictated by the neighbor distribution of p-bits and the adder delays in the hardware. Next, we tested whether overclocking, namely using faster than 15 MHz clocks improves performance or not (FIG. 4a). We define overclocking such that at least some of the updates are not made based on the latest state of the network, similar in spirit to message passing algorithms [59] or the Hogwild!-Gibbs sampling algorithm [33].

Naturally, overclocking the parallel architecture further improves the flips per second obtained from the sIM as shown in Fig. 4a. However, it is critical to check whether these flips are useful or not, since in the overclocked configurations there are no theoretical guarantees for reaching the Boltzmann distribution. To assess the efficacy of the overclocked architecture, we repeat the TTS<sub>99</sub> experiment for the 14-bit factorization problem (399 p-bits) attempting to factor 10 semi-prime numbers 10 times at different clock speeds. Fig. 4b shows that overclocking helps improve TTS<sub>99</sub> up to a critical clock speed of 65 MHz. However, beyond 65 MHz, the TTS starts to increase, indicating many of the flips are not useful to converge to the right answers. The lowest TTS<sub>99</sub> achieved is 0.23 ms at 65 MHz and the corresponding highest effective fps is  $2.59 \times 10^{10}$  for the 14-bit factorization problem. In this specific example, this is a 4.33x improvement over the performance of the timing-satisfying 15 MHz clock. Considering the inexact nature of the overclocked Gibbs sampling, this is a remarkable improvement. Statistical robustness of the inexact Gibbs sampling however, requires careful analysis along the lines of Ref. [60].

The degree of resilience of the system to errors through inexact sampling is an important feature of such probabilistic methods which can be exploited in truly asynchronous nanodevice-based implementations of sIMs [15, 25, 44, 45].

## C. GPU and TPU comparison

Table I summarizes the performance benchmarking of the current work (sIM) with the state-of-the-art GPUs and TPUs. An important distinction between these comparisons is that virtually all optimized implementations of GPUs and TPUs make use of a regular 2D chessboard lattice where partitioning the graph into two color blocks becomes the key piece that enables parallelism. By contrast, in our examples, we show that for realistic instances of combinatorial optimization problems using invertible Boolean circuits, the resulting graphs are sparse but not necessarily regular or bipartite (2-color). Even though theoretical results suggest simple nearest-neighbor models could be sufficient to model any other problem [61], accelerating problem graphs in between nearest-

Platform	Graph	flips/ns
Nvidia Tesla C1060 GPU [57, 58]	Chessboard	7.98
Nvidia Tesla V100 GPU [37]	Chessboard	11.37
Google TPU [37]	Chessboard	12.88
Nvidia Fermi GPU [36]	Chessboard	29.85
FPGA sIM [This work]	Irregular	143.80
Nanodevice sIM [Projected] [15, 25, 44, 45]	Irregular	1,000,000

TABLE I. Comparison of the FPGA-based and nanodevice-based (projected) sIM with optimized GPU and TPU implementations of Markov Chain Monte Carlo sampling. Unlike the GPUs and TPUs, the sIM can support regular chessboard lattices as well as irregular graphs shown in this paper. For the sIM, fps is a size dependent metric as shown in Fig. 2-6. In this table, the best fps achieved in the largest system is quoted.

neighbor and all-to-all will be critically important in practice.

The performance of the sIM flips per second (fps) grows linearly with the number of p-bits in a network, hence the fps becomes a size dependent metric. We observe the sIM reaches up to 143.8 flips/ns at one of the largest graph nodes (4793 p-bits). This is an 18.03x performance gain over the single Nvidia Tesla C1060 GPU with multi-spin coding [57, 58]. It also outperforms the Google Cloud TPU implementation of the 2D Ising model by a factor of 11.17 and its reference Nvidia Tesla V100 GPU by a factor of 12.65 [37]. Furthermore, the sIM provides 4.82x more flips/ns than the Nvidia Fermi GPU coded for simulating the 3D Edwards–Anderson model with parallel tempering [36].

Beyond the FPGA-based sIM implementation we consider in this paper, we make performance projections for massively parallel asynchronous sIMs using nanodevices. Magnetic Tunnel Junctions (MTJ) have recently attracted attention as building blocks for probabilistic computation because of their extreme scalability. The magnetic memory industry have integrated up to billions of single MTJs to replace various parts of the memory hierarchy [62]. Through minimal modifications such MTJs can be made stochastic [15, 63], providing the expensive random number generation with negligible hardware cost. Stochastic MTJs have been demonstrated to provide fast fluctuations ( $\tau = 1$  ns / flip) [44, 45] and at least a million MTJs ( $N = 10^6$ ) can be integrated in massively parallel architectures [15, 25] similar to what we consider in this paper. Following the linear scaling law we demonstrated in Fig. 2, such sIMs can provide  $N/\tau$  flips per second reaching 1 million flips per nanosecond (Table I), provided that the connectivity of the hardware is sparse enough to enable the ideal parallelism demonstrated in this paper.

## VI. EXACT FACTORIZATION OF SEMIPRIMES UP TO 32-BITS

Beyond approximate factorization, we have also performed exact factorization with the sIM. As mention in Section II, we consider the integer factorization problem as a benchmark to compare the performance of our sIM implementation against other probabilistic solvers or D-Wave’s quantum annealers.



### 32-bit Factorization: $4277546633 = 65479 \times 65327$

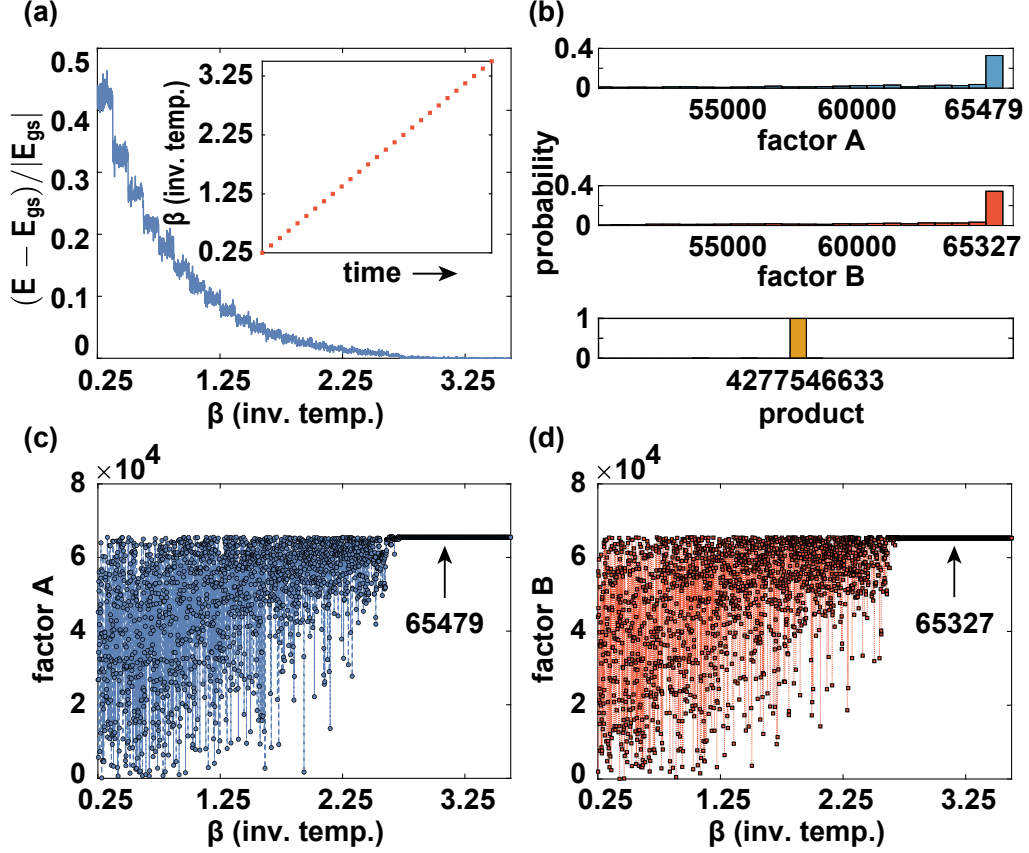


**FIG. 5.** Exact factorization of a 32-bit number,  $P = 4277546633$  in the sIM. (a) The normalized energy as a function of inverse temperature, ( $\beta$  from Eq. (4)). Inset shows the linear annealing schedule. (b) Histograms of the product  $P$  and the factors  $A, B$  over the entire annealing schedule. (c-d) Factors  $A$  and  $B$  at different  $\beta$  values, showing they converge to the right ground state at the highest  $\beta$ .

Platform	Integers Factored (up to)
D-Wave 2000Q [39]	143 (8-bit)
CMOS Inv. Logic [22]	598 (10-bit)
Stochastic MTJ [15]	945 (10-bit)
FPGA RBM [20]	43621 (16-bit)
D-Wave 2000Q [40]	223357 (18-bit)
D-Wave 2000Q [41]	249919 (18-bit)
FPGA sIM [This work]	4277546633 (32-bit)

**TABLE II.** Comparison between the state-of-the-art hardware factorizers and the FPGA-based sIM. Note that all of these solvers treat integer factorization as a frustrated spin-glass problem and perform classical or quantum annealing (or ordinary sampling). We show best reported numbers and single instances, in the case of sIM, random semiprimes up to 32-bits can be reliably factored, see Supplementary Information Section VI.

We found that the sIM can factor random semiprimes up to 32-bits reliably (Supplementary Information, Fig. S7). To the best of our knowledge, this result is by far the best among all other approaches of solving factorization as an optimization problem, for example by D-Wave and others [15, 20, 22, 39–

41]. Table II presents a comparison of integer factorization across the state-of-the-art hardware platforms, and the sIM reports the largest factorization up to 32-bit. What is common to all these solvers is they express factorization as a frustrated spin-glass problem in which the ground state is searched using classical or quantum annealing.

From an algorithm perspective, factorization of 32-bit semiprimes is not difficult since even with trial division this is a relatively easy computation. From a statistical physics perspective, however, finding the doubly degenerate ground state of a frustrated spin glass in a  $2^N$  dimensional space ( $N > 2000$  p-bits) is striking. Contrasting the time to solution shown for approximate factorization (Fig. 3) to that of exact factorization (Fig. S7) as function of problem size, we observe a drastic difference in algorithmic scaling, indicative of a “golf course” like energy landscape where the ground state is well-hidden from “ordinary” approximate states that are easy to reach.

It is worth stressing that we used a simple, standard simulated annealing algorithm without any fine tuning or optimization. Our preliminary findings indicate parallel tempering or other algorithmic methods could improve the success proba-

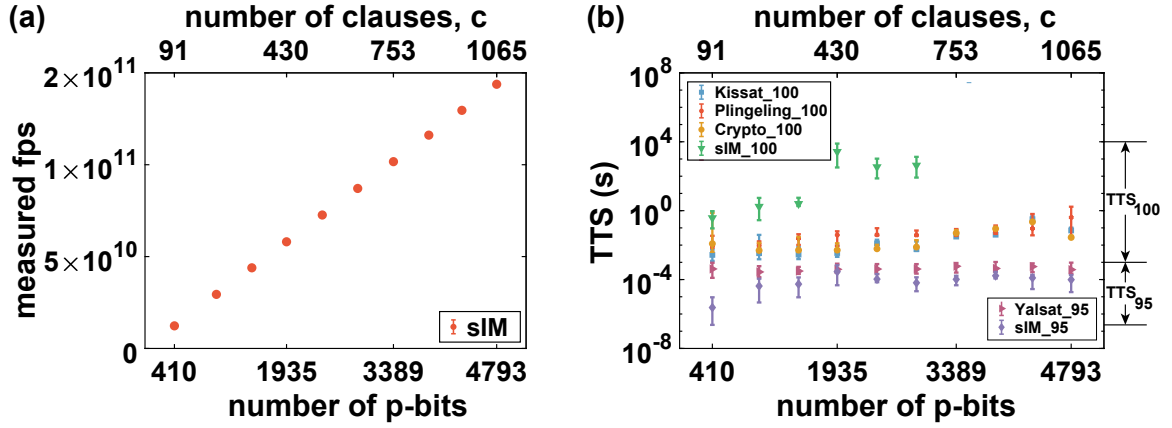


**FIG. 6.** Performance of the sIM vs competition-winning SAT solvers. (a) The flips per second (fps) of the sIM increases linearly with the graph size, showing ideal parallelism. The sIM achieves a record fps of  $1.44 \times 10^{11}$  for the largest problem with 4793 p-bits and 1065 clauses. (b) Runtimes to solve the UBC SATLIB [52] instances. Winning solvers from the SAT 2020 competition, namely Kissat, Plingeling, and, Cryptominisat [64, 65] find 100% solution (all clauses satisfied). SAT competition 2017 random track winner Yalsat [66] is set to find the 95% solution (95% of the clauses satisfied). In exact SAT solving, the sIM is slower than all professional SAT solvers. However, in approximate SAT solving to satisfy 95% of the clauses, the sIM outperforms all of these solvers (including local search-based SAT solvers, such as Yalsat) delivering the fastest solution. The error bars are obtained by taking 100 measurements of fps and TTS for each problem showing the maximum-minimum fluctuations.

bility of these results. We believe the success of our approach over similar alternatives is due to the sparsification methods that have enabled the massively parallel sampling architecture of the sIM.

Fig. 5 presents the exact factorization of a 32-bit number,  $P = 4277546633$ . The linear annealing schedule and the normalized energy of the system are presented in Fig. 5a. The absolute ground state is reached at the coolest temperature (the highest  $\beta$ ). The histograms of the product  $P$  and the factors  $A$ ,  $B$  over the entire annealing schedule are presented in Fig. 5b where the exact factors  $A = 65479$  and  $B = 65327$  are visited reliably. Fig. 5c and Fig. 5d reconfirm that the factors are consistently found at the highest  $\beta$  without any fluctuations.

While we do not show statistics in Fig. 5, in Supplementary Fig. S7, we report the time to find the exact factors ( $TTS_{100}$ ) from 14-bit to 32-bit semiprimes. For any of these problems, the CPU fails to find the exact factors even over a very long time and therefore is excluded from the  $TTS_{100}$  report and we report the sIM times. As before, we attempt to factor 10 different numbers 10 times for each problem.

Unlike approximate factorization where we defined  $TTS_{99}$  as the average time the sIM takes before reaching 99% of the absolute ground state, we find that for exact factoring there is an (empirical) exponential dependence of the time with respect to problem size, in line with the belief that integer factorization is in NP where a known polynomial algorithm does not exist [67]. For 14-bit factorization, the average  $TTS_{100}$  is  $9.60 \times 10^{-3}$  s and for 28-bit factorization, it is 1533.93 s.

To reiterate, extrapolating our observed data with an exponential fit to estimate exact factoring, we find that factorization with this method is not a practical approach in the context of cryptography, in agreement with the observation from Ref. [42]. However, improving SAT solving with massively

parallel hardware could still be useful in accelerating critical subroutines of the best factoring algorithms [43].

## VII. BOOLEAN SATISFIABILITY WITH INVERTIBLE LOGIC

### A. sIM vs competition-winning SAT Solvers

As shown earlier in Fig. 1, it is possible to design invertible Boolean circuits in hardware corresponding to satisfiability instances using the principles of invertible logic. Here, we focus on solving 3SAT problems to demonstrate the hardware acceleration of our massively parallel sIM architecture. In particular, our purpose is to compare the sIM with the best possible software algorithms and we focus on competition winning SAT solvers as a benchmark. As previously, we first report the flips per second (fps) achieved by the sIM for different 3SAT instances defined by the number of their clauses (Fig. 6a). The sIM runs with four parallel and equally phase-shifted clocks operating at 30 MHz since in this case the sparsified graphs require only 4 colors. For the smallest instance ‘uf20-01.cnf’ with 20 variables and 91 clauses, the sIM achieves an fps of  $1.23 \times 10^{10}$  with 410 p-bits. For the largest instance ‘uf250-01.cnf’ with 250 variables and 1065 clauses, the sIM achieves a record fps of  $1.44 \times 10^{11}$  with 4793 p-bit, a 5 to 18x speed up over optimized TPUs and GPUs discussed in Section V (Table I).

Fig. 6b shows the run times to solve the UBC SATLIB [52] instances using different professional SAT solvers and the sIM. We solve each instance 100 times to obtain enough statistics. We compare our results with award-winning solvers from the SAT 2020 competition, namely Kissat, Plingeling, and

Cryptominisat [64, 65]. These conflict-driven clause learning (CDCL) solvers attempt to find the exact solution that satisfies all of the clauses. All these solvers are executed on the same Linux machine having a flagship Intel Core i9-10900 Processor running at up to 5.20 GHz. Time to solve all the clauses (100% solution) is reported as Kissat<sub>100</sub>, Plingeling<sub>100</sub>, and, Crypto<sub>100</sub> respectively. We have used linear simulated annealing in the sIM to report the time to solve all the clauses, labeled as sIM<sub>100</sub> in Fig. 6.

As typical of simulated annealing [56], reaching the absolute ground state is difficult for the sIM. We do report the sIM<sub>100</sub>, namely the time it takes for sIM to satisfy all clauses in a given 3SAT instance and find that despite the enormous number of flips per second taken by the massively parallel processor, we did not find the ground state beyond 2903 bits (Fig. 6, sIM<sub>100</sub>).

In many practical instances however, the user may not be interested in finding the absolute ground state of an optimization problem, and reaching approximate but practically useful solutions as quickly as possible is far more important. In such a paradigm, we find that the sIM beats all of the SAT solvers mentioned (Fig. 6, sIM<sub>100</sub>). Because CDCL-based solvers such as Kissat, Plingeling and Crpytominisat are programmed to find the exact solution, we also test the sIM against another solver Yalsat (2017 SAT competition random track winner) which keeps a current best solution around. We program the solver to stop when it reaches 95% of the solution (denoted as Yalsat<sub>95</sub>). We run Yalsat on the same Linux Machine. sIM is also set to solve 95% of all the clauses and the time to solution is noted as sIM<sub>95</sub>. We find that in this approximate SAT solving mode, the sIM provides the fastest approximate solution outperforming all of the professional SAT solvers by a factor of 4 to 700. We find that there is no failure even for the largest instance ('uf250-01.cnf') we can fit to our FPGA encoded with 4793 p-bits. It takes only 2.36  $\mu$ s for the instance 'uf20-01.cnf' and 98.26  $\mu$ s for the instance 'uf250-01.cnf' to solve 95% of the clauses. We expect larger improvements in more scaled implementations of our sIM architecture using more powerful FPGAs or application specific integrated circuits.

## B. Overclocking to improve SAT solving

Similar to the case of approximate factoring, we test the sIM in an overclocked mode where we try to solve the SAT problem without necessarily performing exact Gibbs sampling. Remarkably, we also find that overclocking (and introducing deliberate simultaneous updates to gain performance improvement) works in the case of SAT solving. In this particular instance, timing is satisfied if the clocks are set to operate at less than 25 MHz and violated otherwise. Fig. 7 shows the overclocked performance of the sIM for the instance 'uf100-01.cnf' with 100 variables and 430 clauses, as a function of individual clock frequencies. As in the case of factorization, we observe a U-shaped behavior: The time to solution (TTS<sub>95</sub>) first improves with increasing clock frequency (despite violating timing and ensuring simultaneous updates are

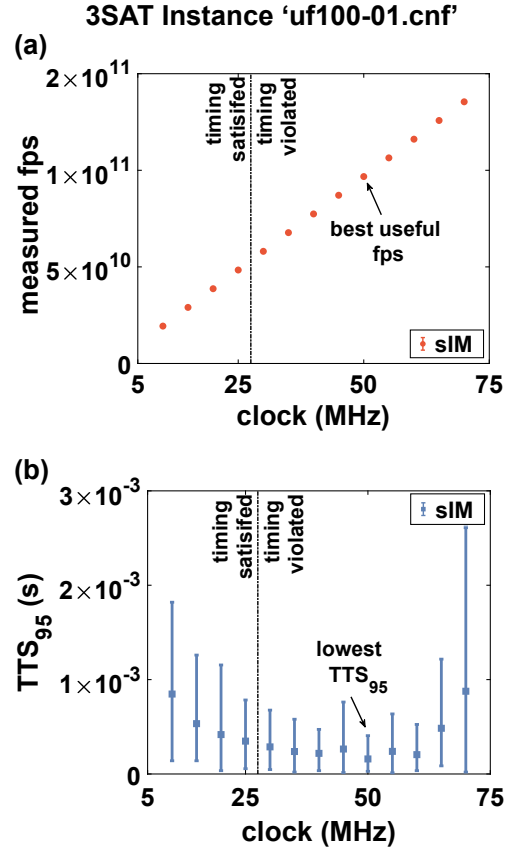


**FIG. 7.** Overclocking to improve SAT solving. (a) For the 3SAT instance 'uf100-01.cnf', measured flips per second plotted as a function of clock frequencies of individual color blocks. Timing is violated above  $\approx 25$  MHz. Based on the results of (b), the highest effective fps is achieved at 50 MHz. (b) Time to solution to satisfy 95% of the clauses, TTS<sub>95</sub> as a function of clock frequencies. Despite errors in timing resulting in simultaneous updates, a lowest TTS is reached at 50 MHz. The error bars are obtained by taking 100 measurements of fps and TTS<sub>95</sub> at each clock speed showing the maximum-minimum fluctuations.

introduced) and then degrades at very high clock frequencies. In this instance with 1935 p-bits, we find that the best useful fps achieved is  $9.68 \times 10^{10}$  at 50 MHz as shown in Fig. 7a. The corresponding lowest TTS<sub>95</sub> reported in Fig. 7b is 159.46  $\mu$ s. This is a 2.18x improvement over the performance of the timing-satisfying 25 MHz clocks. Even though the examples for overclocking in approximate factoring and 3SAT (Fig. 4-7) were for two given instances, the similar behavior they exhibit suggests that overclocking by introducing deliberate errors to improve performance can be a further method of extracting more performance out of massively parallel sIMs.

One reason why overclocking seems to improve performance significantly could be due to the slowing down of the network dynamics at lower temperatures (higher  $\beta$ ). At the end of an annealing schedule, despite failing to compute individual p-bit inputs ( $I_i$ ) exactly through Eq. (2), errors may not be significant because p-bits do not change their states frequently. We believe that scaled implementations with truly



asynchronous building blocks could exploit the resilience of such probabilistic systems even further.

## VIII. CONCLUSIONS

In this paper, we proposed and implemented a massively parallel stochastic processing unit (sIM) to parallelize a broad range of Markov Chain Monte Carlo (MCMC) algorithms useful for computationally hard problems. In particular, overcoming the fundamentally serial nature of MCMC algorithms such as Gibbs sampling, we have shown an architecture that can achieve ideal parallelism where the main metric of the sIM, the flips per second, scales linearly with the number of probabilistic bits in the system. This parallel architecture used several algorithmic ideas of combining invertible logic to produce sparse graph representations of combinatorial optimization problems such as Boolean satisfiability and integer factorization. Further sparsification was needed to ensure matrix multiplication and addition can be performed before independent p-bits are updated. The architecture used approximate graph coloring to parallelize sampling.

We have shown a moderate FPGA-based implementation of this concept where we have achieved three major results. First, comparisons to an ordinary CPU implementation of Gibbs sampling showed that the sIM is able to achieve up to 6-orders improvement in flips per second, which directly translated to advantages in time to solution in the integer factorization problem. Comparisons to highly optimized GPU and TPU implementations, the sIM showed up to 5-18x measured speed up in flips per second, without the use of regular or simple graphs as commonly used for benchmarking purposes in GPUs and CPUs. Second, the sIM was able to factor semiprimes up to 32-bit integers, far larger than the best available results on factoring where an optimization approach is taken. And third, the sIM was able to beat competition winning SAT solvers in approximate satisfiability, delivering superior performance compared to the best possible classical approach in solving satisfiability problems. We have also shown how overclocking in the spirit of asynchronous Gibbs sampling [33] could lead to performance improvements despite the lack of theoretical guarantees in reaching the expected final distributions.

These results were obtained in a FPGA platform where our problem sizes were limited to the number of probabilistic bits we could fit in a single device. Use of more powerful FPGAs would immediately extend the size of problems programmable to the sIM. The ideal parallelism we achieved in the architecture, coupled with algorithmic sparsification techniques we developed can further be exploited in highly scaled implementations. In particular, nanodevice (or analog CMOS-based) p-bits can produce significant improvements over our present results, as the search for domain-specific hardware in the beyond Moore era of electronics intensifies.

## IX. METHODS

### A. Simulated annealing

In simulated annealing,  $\beta$  is gradually increased over time. According to Eq. 2, multiplication of  $\beta$  and the input weights ( $J, h$ ) are performed in MATLAB. The updated values of  $J$  and  $h$  are sent to the FPGA for every  $\beta$  over time to do simulated annealing.

### B. Data READ/WRITE

MATLAB is used to READ/WRITE data from the FPGA through a USB-JTAG interface. A programmable timer is implemented in the FPGA. Using the timer, a global DISABLE signal is sent to the p-bits before a READ instruction. The timer is preset from the program (MATLAB) and all the p-bits are automatically frozen at the same time when the time is up. Once the p-bits are frozen, the data are READ using the USB-JTAG interface and sent to MATLAB for post-processing. When the READ instruction is DONE, the timer is RESET from MATLAB to resume the p-bits if necessary. Similarly, for the WRITE instruction, a global DISABLE signal is sent using the programmable timer to freeze the p-bits before sending the weights. Likewise the READ instruction, the timer is RESET from MATLAB to resume the p-bits after the WRITE instruction is DONE.

### C. Measurement of fps

Each p-bit is designed with a programmable stopwatch counter in the FPGA. A global counter running parallelly is set to count up to a preset value at the positive edge of a known clock. When the global counter is DONE counting, a global DISABLE signal is broadcast to all other counters. Comparing the p-bit counter outputs (number of flips) with the global counter preset value, the time for the total flips is obtained. With this data, the fps of the sIM is measured experimentally for each p-bit. To measure the fps in the case of the CPU, built-in functions from MATLAB is used to measure the elapsed time and programmatically count the total flips in that time. With this data, the fps is measured in real-time.

### D. Measurement of TTS

In the FPGA, a minimum time is set using the programmable timer to find the solution to the problem of interest. After that time, a global DISABLE signal is sent to READ the latest TTS. In iterations, the minimum time is incremented, and the p-bits are RESET. This process is repeated until the desired solution is reached. The latest TTS is reported as the TTS of the sIM for that problem. In measuring the TTS, we do not include the READ/WRITE times through the USB-JTAG interface. While we use a slow USB-JTAG

interface (up to 33 MHz) for the convenience of using MATLAB, much faster R/W protocols such as PCI Express (up to 8 Gb/s) would remove this time entirely. To measure the TTS in the case of the CPU, a predefined minimum number of samples is set to find the solution. The number of samples is increased in iterations until the optimum solution is found by the CPU. The time to solution is recorded using the built-in function and the latest one is reported as TTS of the CPU for that problem.

### E. Setting up the SAT solvers

The online source codes of the SAT solvers are used to build the solvers on a Linux machine. For the CDCL SAT solvers, the time to find the 100% solution is measured using a simple Python script. For the local SAT solver Yalsat, the program is set to report the TTS for the current best solution.

### ACKNOWLEDGMENTS

The authors are grateful to Brian M. Sutton for fruitful discussions and detailed comments on an earlier version of this manuscript. It is a pleasure to acknowledge Xilinx for hardware support. K.Y.C. and L.T. acknowledge support from the Institute of Energy Efficiency, UC Santa Barbara. The research of A.G., M.C., and G.F. has been supported by Petaspin association ([www.petaspin.com](http://www.petaspin.com)). G.F. also acknowledges support from MARIS (<https://www.maris-ricerca.it/>). Use was made of computational facilities purchased with funds from the National Science Foundation (CNS-1725797) and administered by the Center for Scientific Computing (CSC). The CSC is supported by the California NanoSystems Institute and the Materials Research Science and Engineering Center (MRSEC; NSF DMR 1720256) at UC Santa Barbara.

### REFERENCES

- [1] N. Metropolis, A. W. Rosenbluth, M. N. Rosenbluth, A. H. Teller, and E. Teller, Equation of state calculations by fast computing machines, *The journal of chemical physics* **21**, 1087 (1953).
- [2] A. Buluc, T. G. Kolda, S. M. Wild, M. Anitescu, A. DeGennaro, J. Jakeman, C. Kamath, M. E. Lopes, P.-G. Martinsson, K. Myers, *et al.*, Randomized algorithms for scientific computing (rasc), arXiv preprint arXiv:2104.11079 (2021).
- [3] G. E. Hinton, A practical guide to training restricted boltzmann machines, in *Neural networks: Tricks of the trade* (Springer, 2012) pp. 599–619.
- [4] V. K. Mansinghka, E. M. Jonas, and J. B. Tenenbaum, Stochastic digital circuits for probabilistic inference, *Massachusetts Institute of Technology, Technical Report MITCSAIL-TR 2069* (2008).
- [5] A. Bouchard-Côté, S. J. Vollmer, and A. Doucet, The bouncy particle sampler: A nonreversible rejection-free markov chain monte carlo method, *Journal of the American Statistical Association* **113**, 855 (2018).
- [6] W. Krauth, Quantum monte carlo calculations for a large number of bosons in a harmonic trap, *Physical review letters* **77**, 3695 (1996).
- [7] S. Kirkpatrick, C. D. Gelatt Jr, and M. P. Vecchi, Optimization by simulated annealing, in *Readings in Computer Vision* (Elsevier, 1987) pp. 606–615.
- [8] P. L. McMahon et al., A fully programmable 100-spin coherent ising machine with all-to-all connections, *Science* **354**, 614 (2016).
- [9] M. Yamaoka, C. Yoshimura, M. Hayashi, T. Okuyama, H. Aoki, and H. Mizuno, 24.3 20k-spin ising chip for combinatorial optimization problem with cmos annealing, in *2015 IEEE International Solid-State Circuits Conference-(ISSCC) Digest of Technical Papers* (IEEE, 2015) pp. 1–3.
- [10] H. Goto, K. Tatsumura, and A. R. Dixon, Combinatorial optimization by simulating adiabatic bifurcations in nonlinear hamiltonian systems, *Science advances* **5**, eaav2372 (2019).
- [11] T. Wang and J. Roychowdhury, Oim: Oscillator-based ising machines for solving combinatorial optimisation problems, in *International Conference on Unconventional Computation and Natural Computation* (Springer, 2019) pp. 232–256.
- [12] I. Ahmed, P.-W. Chiu, and C. H. Kim, A probabilistic self-annealing compute fabric based on 560 hexagonally coupled ring oscillators for solving combinatorial optimization problems, in *2020 IEEE Symposium on VLSI Circuits* (IEEE, 2020) pp. 1–2.
- [13] J. Chou, S. Bramhavar, S. Ghosh, and W. Herzog, Analog coupled oscillator based weighted ising machine, *Scientific reports* **9**, 1 (2019).
- [14] S. Dutta, A. Khanna, A. Assoa, H. Paik, D. Schlom, Z. Toroczkai, A. Raychowdhury, and S. Datta, An ising hamiltonian solver based on coupled stochastic phase-transition nano-oscillators, *Nature Electronics* **4**, 502 (2021).
- [15] W. A. Borders et al., Integer factorization using stochastic magnetic tunnel junctions, *Nature* (2019).
- [16] M. Baity-Jesi, R. A. Baños, A. Cruz, L. A. Fernandez, J. M. Gil-Narvió, A. Gordillo-Guerrero, D. Iñiguez, A. Maiorano, F. Mantovani, E. Marinari, *et al.*, Janus ii: A new generation application-driven computer for spin-system simulations, *Computer Physics Communications* **185**, 550 (2014).
- [17] M. Aramon, G. Rosenberg, E. Valiante, T. Miyazawa, H. Tamura, and H. G. Katzgraber, Physics-inspired optimization for quadratic unconstrained problems using a digital annealer, *Frontiers in Physics* **7**, 48 (2019).
- [18] K. Yamamoto, K. Ando, N. Mertig, T. Takemoto, M. Yamaoka, H. Teramoto, A. Sakai, S. Takamaeda-Yamazaki, and M. Motomura, 7.3 statica: A 512-spin 0.25 m-weight full-digital annealing processor with a near-memory all-spin-updates-at-once architecture for combinatorial optimization with complete spin-spin interactions, in *2020 IEEE International Solid-State Circuits Conference-(ISSCC)* (IEEE, 2020) pp. 138–140.
- [19] S. Patel, L. Chen, P. Canoz, and S. Salahuddin, Ising model optimization problems on a fpga accelerated restricted boltzmann machine, arXiv preprint arXiv:2008.04436 (2020).
- [20] S. Patel et al., Logically synthesized, hardware-accelerated, restricted boltzmann machines for combinatorial optimization and integer factorization, arXiv preprint arXiv:2007.13489 (2020).
- [21] Y. Su, J. Mu, H. Kim, and B. Kim, A 252 spins scalable cmos ising chip featuring sparse and reconfigurable spin interconnects for combinatorial optimization problems, in *2021 IEEE Custom Integrated Circuits Conference (CICC)* (IEEE, 2021) pp. 1–2.

- [22] S. Smithson et al., Efficient cmos invertible logic using stochastic computing, *IEEE Transactions on Circuits and Systems I: Regular Papers* **66**, 2263 (2019).
- [23] F. Cai, S. Kumar, T. Van Vaerenbergh, X. Sheng, R. Liu, C. Li, Z. Liu, M. Foltin, S. Yu, Q. Xia, *et al.*, Power-efficient combinatorial optimization using intrinsic noise in memristor hopfield neural networks, *Nature Electronics* **3**, 409 (2020).
- [24] K. Tatsumura, M. Yamasaki, and H. Goto, Scaling out ising machines using a multi-chip architecture for simulated bifurcation, *Nature Electronics* **4**, 208 (2021).
- [25] B. Sutton et al., Autonomous probabilistic coprocessing with petaflips per second, *IEEE Access* **8**, 157238 (2020).
- [26] D. H. Ackley, G. E. Hinton, and T. J. Sejnowski, A learning algorithm for boltzmann machines, *Cognitive science* **9**, 147 (1985).
- [27] G. E. Hinton, Boltzmann machine, *Scholarpedia* **2**, 1668 (2007).
- [28] V. Dixit, R. Selvarajan, M. A. Alam, T. S. Humble, and S. Kais, Training restricted boltzmann machines with a d-wave quantum annealer, *Front. Phys.* **9**: 589626. doi: 10.3389/fphy (2021).
- [29] Y. Koshka and M. A. Novotny, Toward sampling from undirected probabilistic graphical models using a d-wave quantum annealer, *Quantum Information Processing* **19**, 1 (2020).
- [30] D. Koller and N. Friedman, *Probabilistic graphical models: principles and techniques* (MIT press, 2009).
- [31] K. Y. Camsari et al., Stochastic p-bits for invertible logic, *Physical Review X* **7**, 031014 (2017).
- [32] J. Gonzalez, Y. Low, A. Gretton, and C. Guestrin, Parallel gibbs sampling: From colored fields to thin junction trees, in *Proceedings of the Fourteenth International Conference on Artificial Intelligence and Statistics (JMLR Workshop and Conference Proceedings, 2011)* pp. 324–332.
- [33] M. J. Johnson, J. Saunderson, and A. Willsky, Analyzing hogwild parallel gaussian gibbs sampling, *Advances in neural information processing systems* **26**, 2715 (2013).
- [34] S. Geman and D. Geman, Stochastic relaxation, gibbs distributions, and the bayesian restoration of images, *IEEE Transactions on pattern analysis and machine intelligence* , 721 (1984).
- [35] G. G. Ko, Y. Chai, R. A. Rutenbar, D. Brooks, and G.-Y. Wei, Flexgibbs: Reconfigurable parallel gibbs sampling accelerator for structured graphs, in *2019 IEEE 27th Annual International Symposium on Field-Programmable Custom Computing Machines (FCCM)* (IEEE, 2019) pp. 334–334.
- [36] Y. Fang, S. Feng, K.-M. Tam, Z. Yun, J. Moreno, J. Ramanujam, and M. Jarrell, Parallel tempering simulation of the three-dimensional edwards–anderson model with compact asynchronous multispin coding on gpu, *Computer Physics Communications* **185**, 2467 (2014).
- [37] K. Yang, Y.-F. Chen, G. Roumpos, C. Colby, and J. Anderson, High performance monte carlo simulation of ising model on tpu clusters, in *Proceedings of the International Conference for High Performance Computing, Networking, Storage and Analysis* (2019) pp. 1–15.
- [38] M. Ghaffari and C. Lymouri, Simple and near-optimal distributed coloring for sparse graphs, *arXiv preprint arXiv:1708.06275* (2017).
- [39] E. Andriyash et al., Boosting integer factoring performance via quantum annealing offsets, *D-Wave Technical Report Series* **14** (2016).
- [40] R. Dridi and H. Alghassi, Prime factorization using quantum annealing and computational algebraic geometry, *Scientific reports* **7**, 1 (2017).
- [41] S. Jiang, K. A. Britt, A. J. McCaskey, T. S. Humble, and S. Kais, Quantum annealing for prime factorization, *Scientific reports* **8**, 1 (2018).
- [42] M. Mosca et al., Factoring semi-primes with (quantum) solvers, *arXiv preprint arXiv:1902.01448* (2019).
- [43] M. Mosca, J. M. V. Basso, and S. R. Verschoor, On speeding up factoring with quantum sat solvers, *Scientific Reports* **10**, 1 (2020).
- [44] C. Safranski, J. Kaiser, P. Trouilloud, P. Hashemi, G. Hu, and J. Z. Sun, Demonstration of nanosecond operation in stochastic magnetic tunnel junctions, *Nano Letters* **21**, 2040 (2021).
- [45] K. Hayakawa, S. Kanai, T. Funatsu, J. Igarashi, B. Jinnai, W. Borders, H. Ohno, and S. Fukami, Nanosecond random telegraph noise in in-plane magnetic tunnel junctions, *Physical Review Letters* **126**, 117202 (2021).
- [46] D. Bréaz, New methods to color the vertices of a graph, *Communications of the ACM* **22**, 251 (1979).
- [47] N. Onizawa, K. Nishino, S. Smithson, B. Meyer, W. Gross, H. Yamagata, H. Fujita, and T. Hanyu, A design framework for invertible logic, in *2019 53rd Asilomar Conference on Signals, Systems, and Computers* (IEEE, 2019) pp. 312–316.
- [48] J. Biamonte, Nonperturbative k-body to two-body commuting conversion hamiltonians and embedding problem instances into ising spins, *Physical Review A* **77**, 052331 (2008).
- [49] A. Z. Pervaiz, L. A. Ghantasala, K. Y. Camsari, and S. Datta, Hardware emulation of stochastic p-bits for invertible logic, *Scientific reports* **7**, 10994 (2017).
- [50] F. L. Traversa and M. Di Ventra, Polynomial-time solution of prime factorization and np-complete problems with digital memcomputing machines, *Chaos: An Interdisciplinary Journal of Nonlinear Science* **27**, 023107 (2017).
- [51] S. Arora and B. Barak, *Computational complexity: a modern approach* (Cambridge University Press, 2009).
- [52] H. H. Hoos and T. Stützle, Satlib: An online resource for research on sat, *Sat* **2000**, 283 (2000).
- [53] A. Lucas, Ising formulations of many np problems, *Frontiers in Physics* **2**, 5 (2014).
- [54] W. M. Kaminsky and S. Lloyd, Scalable architecture for adiabatic quantum computing of np-hard problems, *Quantum computing and quantum bits in mesoscopic systems* , 229 (2004).
- [55] V. Choi, Minor-embedding in adiabatic quantum computation: I. the parameter setting problem, *Quantum Information Processing* **7**, 193 (2008).
- [56] E. Aarts and J. Korst, *Simulated annealing and Boltzmann machines: a stochastic approach to combinatorial optimization and neural computing* (John Wiley & Sons, Inc., 1989).
- [57] B. Block, P. Virnau, and T. Preis, Multi-gpu accelerated multi-spin monte carlo simulations of the 2d ising model, *Computer Physics Communications* **181**, 1549 (2010).
- [58] T. Preis, P. Virnau, W. Paul, and J. J. Schneider, Gpu accelerated monte carlo simulation of the 2d and 3d ising model, *Journal of Computational Physics* **228**, 4468 (2009).
- [59] M. Mezard and A. Montanari, *Information, physics, and computation* (Oxford University Press, 2009).
- [60] X. Zhang, R. Bashizade, Y. Wang, S. Mukherjee, and A. R. Lebeck, Statistical robustness of markov chain monte carlo accelerators, in *Proceedings of the 26th ACM International Conference on Architectural Support for Programming Languages and Operating Systems* (2021) pp. 959–974.
- [61] G. De las Cuevas and T. S. Cubitt, Simple universal models capture all classical spin physics, *Science* **351**, 1180 (2016).
- [62] S. Bhatti, R. Sbiaa, A. Hirohata, H. Ohno, S. Fukami, and S. Piramanayagam, Spintronics based random access memory: a review, *Materials Today* **20**, 530 (2017).
- [63] K. Kobayashi, W. A. Borders, S. Kanai, K. Hayakawa, H. Ohno, and S. Fukami, Sigmoidal curves of stochastic magnetic tunnel



- junctions with perpendicular easy axis, *Applied Physics Letters* **119**, 132406 (2021).
- [64] A. B. K. F. M. Fleury and M. Heisinger, Cadical, kissat, para-cooba, plingeling and treengeling entering the sat competition 2020, *SAT COMPETITION 2020*, 50 (2020).
- [65] M. Soos, J. Devriendt, S. Gocht, A. Shaw, and K. S. Meel, Cryptominisat with ccanr at the sat competition 2020, *SAT COMPETITION 2020*, 27 (2020).
- [66] A. Biere, Cadical, lingeling, plingeling, treengeling and yalsat entering the sat competition 2017, *Proceedings of SAT Competition*, 14 (2017).
- [67] A. K. Lenstra, H. W. Lenstra Jr, M. S. Manasse, and J. M. Pollard, The number field sieve, in *Proceedings of the twenty-second annual ACM symposium on Theory of computing* (1990) pp. 564–572.
- [68] R. Faria, K. Y. Camsari, and S. Datta, Implementing bayesian networks with embedded stochastic mram, *AIP Advances* **8**, 045101 (2018).
- [69] airhdl.com, airhdl VHDL/SystemVerilog Register Generator, <https://airhdl.com>.
- [70] D. Blackman and S. Vigna, Scrambled linear pseudorandom number generators, *arXiv preprint arXiv:1805.01407* (2018).
- [71] M. Matsumoto and T. Nishimura, Mersenne twister: a 623-dimensionally equidistributed uniform pseudo-random number generator, *ACM Transactions on Modeling and Computer Simulation (TOMACS)* **8**, 3 (1998).
- [72] M. Suzuki, Relationship between d-dimensional quantal spin systems and (d+ 1)-dimensional ising systems: Equivalence, critical exponents and systematic approximants of the partition function and spin correlations, *Progress of theoretical physics* **56**, 1454 (1976).

## SUPPLEMENTARY INFORMATION

### F. Characteristics of CMOS and nanodevice based p-bits

In Section I of the main paper, we have discussed Eq. 3 of a p-bit that can be implemented in several hardware platforms. A CMOS implementation of Eq. 3 is presented in Supplementary Fig. S1a. A clock-triggered random number generator (RNG) provides the  $\text{rand}_U(-1, 1)$  function and a lookup table (LUT) maps the tanh activation function. Finally, a comparator is used to trigger the flip of the p-bit. The input-output characteristics of a CMOS implemented p-bit is shown in Supplementary Fig. S1b. Eq. 3 can also be implemented using nanodevices such as a 14-nm FinFET and a stochastic MTJ where a mapping between the dimensionless Eq. 3 and the device characteristics can be made [68]. The nanodevice circuit and its input-output characteristics are presented in Supplementary Fig. S1c,d.

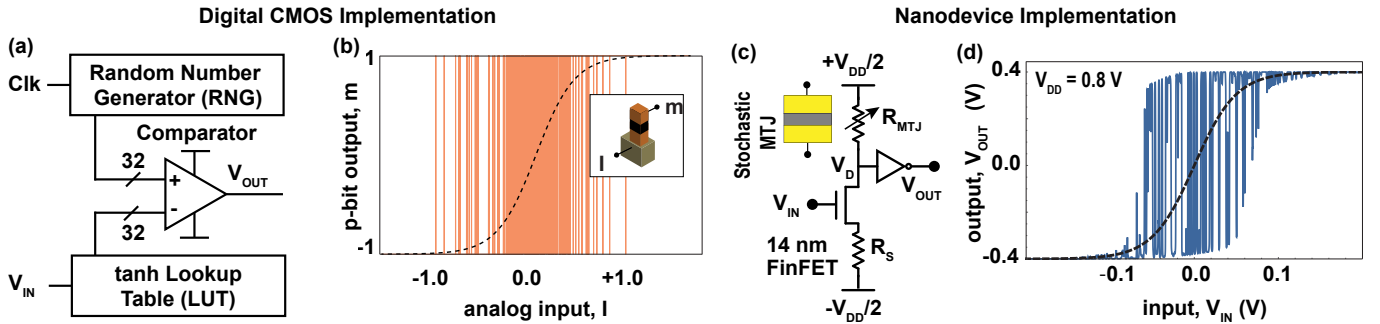


**FIG. S1.** (a) Digital CMOS implementation of Eq. 3 of a p-bit using an RNG, a LUT, and a comparator. (b) Input-output characteristics of the digital CMOS p-bit. (c) Nanodevice implementation of Eq. 3 using a 14 nm FinFET and a stochastic MTJ. (d) Input-output characteristics of the nanodevice p-bit.

### G. FPGA implementation of the sIM

We have presented the experimental results of the sIM in the main paper without technical details about the implementation of the architecture. Here, we discuss an FPGA based implementation of the sIM in a Xilinx Virtex UltraScale+ VCU118 Evaluation board. The basic architecture of the FPGA design is presented in Supplementary Fig. S2.

#### 1. Interfacing unit

We use MATLAB as an Advanced eXtensible Interface (AXI) master to communicate with the slave FPGA board through a USB-JTAG interface (Supplementary Fig. S2a). We have designed an AXI master integrated IP on the board that transfers data

with a 32-bit memory-mapped slave register IP via the fourth generation AXI (AXI4) protocol. An external website ‘airhdl’ [69] is used to manage the memory mapping of the registers.

## 2. Clocking unit

Section IV in the main paper explains how approximate graph coloring can be used to color p-bit blocks for massive parallelism. For this, we have used built-in clocks on the FPGA board to drive the LFSRs inside the p-bit blocks as shown in (Supplementary Fig. S2b). A 250 MHz Low-voltage Differential Signaling (LVDS) system clock generates equally phase-shifted and parallel stable clocks using the on-board Mixed-Mode Clock Manager (MMCM) Module. This module is available in the VCU118 LogiCORE IP provided by Xilinx. The generated clocks are very accurate, have minimum jitter and minor phase error. The colored p-bit blocks get triggered with these phase-shifted clocks.

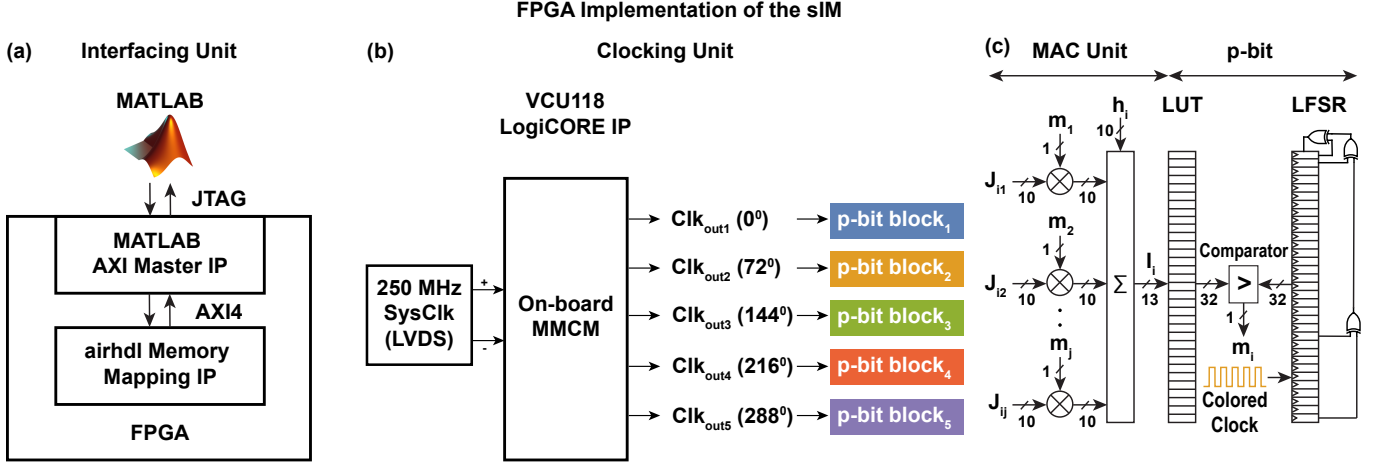


**FIG. S2.** FPGA based implementation of the sIM. (a) An interfacing unit to communicate between MATLAB the FPGA. (b) A built-in clocking unit to generate equally phase-shifted parallel clocks to trigger the colored p-bit blocks. (c) The MAC unit to implement Eq. 2 where the colored clock from the general architecture is fed into the LFSR of the p-bit.

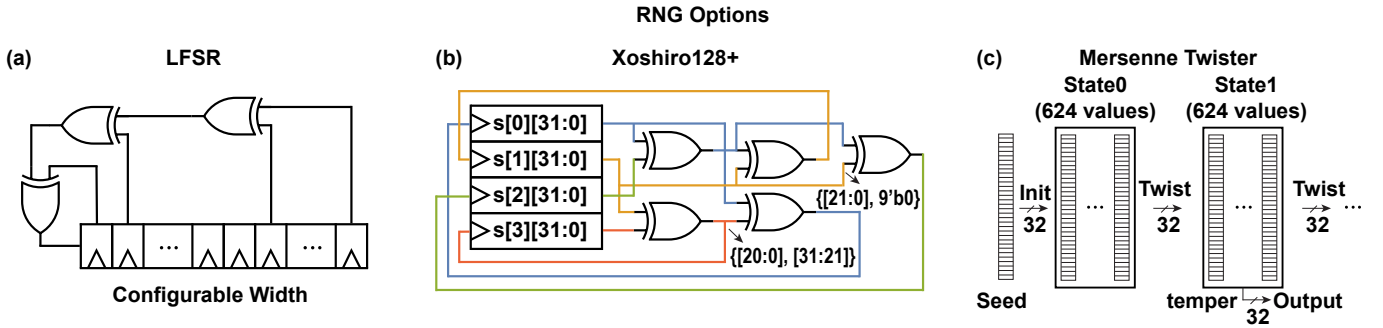


**FIG. S3.** Different reconfigurable RNG options in the sIM. (a) A linear-feedback shift register (LFSR) with programmable bit-width. (b) A Xoshiro128+ [70] RNG. (c) A Mersenne Twister [71].

## 3. MAC unit

In Section II of the main paper, we described the MAC unit interconnecting the p-bits and computing Eq. (2). Fig. S2c illustrates the MAC unit implemented in the FPGA. In this work, we have used 32-bit linear-feedback shift registers (LFSRs) as RNGs after extensive experiments with different types of RNGs with different bit-widths. Supplementary Fig. S3 presents some of the RNG options, namely LFSR, Xoshiro128+ [70], and the Mersenne Twister [71]. The sIM is reconfigurable to choose any of these RNGs and change the bit-width. The LUT bit-width is reconfigurable accordingly and a comparator compares the

outputs of the LUT and the LFSR. The input weights  $(J, h)$  are programmable and we multiply them by  $\beta$  from the MATLAB level to implement simulated annealing.

### H. Correspondence between binary and bipolar variables

Eq. 1-3 presented in Section I of the main paper use bipolar variables. It is more convenient to use binary variables for the FPGA-based implementation of the sIM. In the MAC unit, all the variables are calculated using binary notations where the final output for a p-bit is  $m_i \in [0, 1]$ . The bipolar to binary conversion is done using the following equations,

$$J_{\text{binary}} = 2 \times J_{\text{bipolar}} \quad (\text{S.1})$$

$$h_{\text{binary}} = h_{\text{bipolar}} - J_{\text{bipolar}} \mathbb{A} \quad (\text{S.2})$$

where,  $\mathbb{A}$  is an  $[N \times 1]$  vector of ones, and  $N$  is the number of p-bits. We convert the tanh function in the LUT from bipolar to binary using the following transformation,

$$z = \frac{1 + \tanh}{2} \quad (\text{S.3})$$

### I. Basic logic gates for probabilistic computing

Section III of the main paper illustrates how any invertible logic probabilistic circuit can be composed using basic logic gates and full adders to solve combinatorial optimization problems. Supplementary Fig. S4a-l presents the basic logic gates (COPY/NOT/AND/OR) used to build such p-circuits. The  $J$  and  $h$  matrices have few unique weights that are highlighted using unique colors. The energy plot corresponding to the Boltzmann probability are also included in the figure. For example, the AND gate has three p-bits and its lowest energy states show that  $[m_1 \ m_2 \ m_3] = \{000, 010, 100, 111\}_{\text{bin}}$  are being emphasized which agrees with the truth table of the AND gate. Supplementary Fig. S4m-o further illustrates how to compose an invertible logic p-circuit using these basic logic gates (see Section S J for the mathematical justification). The composite circuit combines the  $[3 \times 3]$   $J$  matrices of the AND and OR gates which become a  $[5 \times 5]$  matrix after fusion of the common node. Similarly, it combines the  $[3 \times 1]$   $h$  matrices of the AND and the OR gates which become a  $[5 \times 1]$   $h$  matrix after fusion. The energy plot reveals that the lowest energy states  $[m_1 \ m_2 \ m_3 \ m_4] = \{0001, 0101, 1001, 1110, 1111\}_{\text{bin}}$  are being emphasized when  $m_5 = 1$ , which agrees with the truth table of the composite circuit.

### J. Fusion and Sparsification

In this section, our objective is to define two graph modification techniques we call fusion and sparsification. Fusion refers to combining multiple inputs as in Fig. S5a to a single node as in Fig. S5b. Sparsification refers to splitting a node into multiple p-bits to decrease the vertex degree (number of neighbors) of a given node as in Fig. S5c. In this section, we first give a mathematical proof of the equivalence between a fused and sparsified circuit and then we give analytical expressions for the size of the sparsified circuits to quantify the number of extra p-bits added.

#### 1. Mathematical equivalence of fused and sparsified graphs

Here, we would like to establish that as the annealing parameter  $\beta$  of Eq. 3 (main paper) is increased ( $\beta \rightarrow \infty$  at the end of an annealing schedule), the sparsified and the fused circuits have the same ground state for a given optimization problem. The connection between the sparsification and the fusion also allows a natural way of composing p-circuits which we elaborate next. Suppose there are two subcircuits we are trying to connect in which  $m_A$  corresponds to the node from subcircuit A and  $m_B$  corresponds to the node from subcircuit B and that  $m_A$  and  $m_B$  need to be tied together. Both these systems are described by their respective energies (ignoring biases without loss of generality):

$$E_A = - \left( \sum_{\substack{i \neq A \\ i < j}} J_{ij} m_i m_j + \sum_j J_{Aj} m_j m_A \right) \quad (\text{S.4})$$

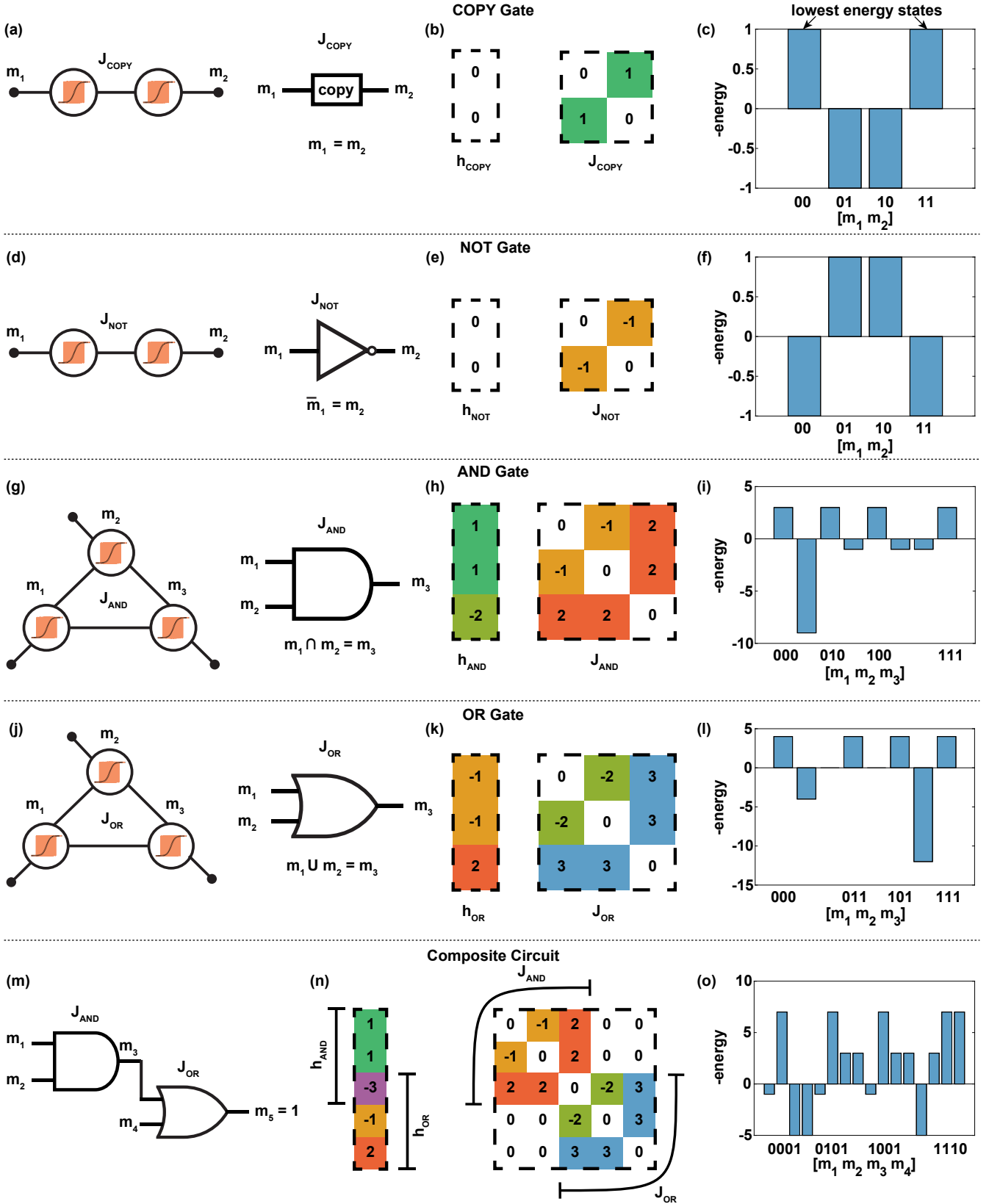


**FIG. S4.** Basic logic gates for probabilistic computing. (a)-(l) COPY/NOT/AND/OR gates with  $J$  and  $h$  matrices having few unique weights highlighted using unique colors (not to be confused with graph coloring). The lowest energy states match the basic truth tables where the vectors  $[m_1 \ m_2]$  or  $[m_1 \ m_2 \ m_3]$  are represented by the corresponding binary numbers. (m)-(o) A composite p-circuit built using an AND gate and an OR gate, its  $J$  and  $h$  matrices and the energy plot. Note that unlike the other examples,  $m_5$  is clamped to 1 in this example.



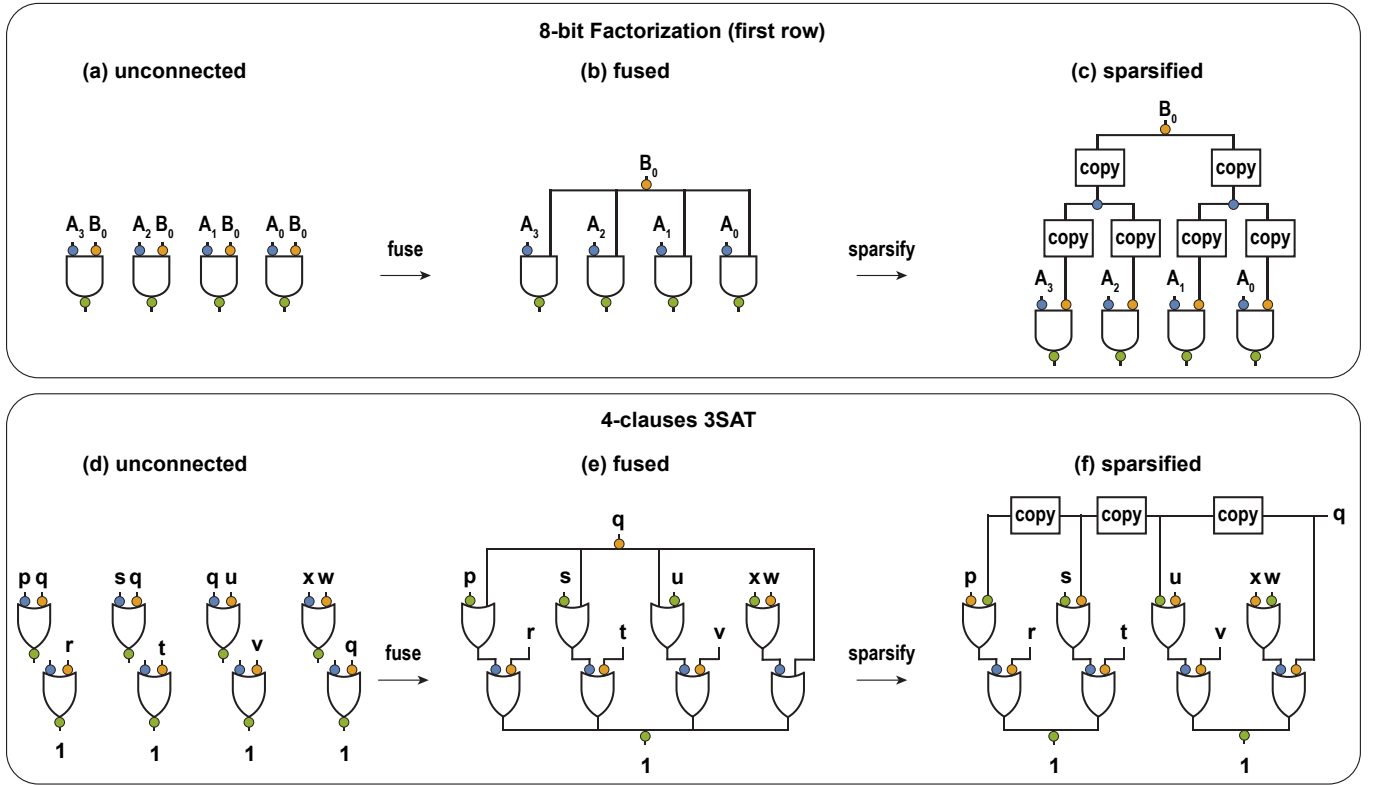


**FIG. S5.** Fusion and sparsification techniques for probabilistic gates (all the gates shown in this figure are probabilistic version of ordinary Boolean gates as shown in FIG. S4). (a) An unconnected 8-bit factorizer has 4 p-bits for  $B_0$ . (b) Fused version of the 8-bit factorizer has only one p-bit for  $B_0$ . (c) Sparsified 8-bit factorizer has 7 p-bits for  $B_0$ . (d) An unconnected 4-clauses 3SAT solver circuit has 4 p-bits for input 'q' and 4 p-bits for the outputs. (e) Fused version of the 3SAT solver has only 1 p-bit for 'q' and 1 p-bit for the output. (f) Sparsified 3SAT solver has 4 p-bits for 'q' and 2 p-bits for the outputs.

$$E_B = - \left( \sum_{\substack{i \neq B \\ i < j}} J'_{ij} m_i m_j + \sum_j J'_{Bj} m_j m_B \right) \quad (\text{S.5})$$

where we separated the energy terms corresponding to  $m_A$  and  $m_B$  from the rest of the subcircuits. If  $m_A$  and  $m_B$  are to be connected as a common node between these subcircuits, as in ordinary digital circuits, a positive interaction parameter (ferromagnetic,  $J_T > 0$ ) can be used to connect them such that the total energy of the composed system is given as:

$$E = E_A + E_B - J_T m_A m_B \quad (\text{S.6})$$

This situation corresponds to the sparsified network where the interaction parameter  $J_T$  corresponds to the COPY gate which ties the same logical value to  $m_A$  and  $m_B$ .

We continue the analysis with a physical observation. As the temperature is lowered ( $\beta \rightarrow \infty$ ),  $m_A$  and  $m_B$  cannot differ in their states due to the large energy penalty incurred by  $\beta J_T$ , or mathematically,  $P(m_A \neq m_B) = \exp(-\beta J_T) \rightarrow 0$ , independent of the specific value of  $J_T$ . This allows, in the bipolar notation where  $m_A, m_B \in \pm 1$ , the following trick:  $m_A = m_B$  and  $m_A^2 = 1$ . This means that the last term in Eq. (S.6) becomes a constant and drops out of the final Boltzmann probabilities since any constant term in the energy cancels out:

$$P(m_1, \dots, m_N) = \frac{1}{Z} \exp(\beta J_T) \exp[-\beta(E_A + E_B)] \quad (\text{S.7})$$

where

$$Z = \sum \exp(-\beta E) = \exp(\beta J_T) \sum \exp -\beta(E_A + E_B) \quad (\text{S.8})$$

This analysis indicates that for an annealed system, irrespective of the strength of the coupling parameter  $J_T$ , there is no difference in the final probabilities between subcircuits A and B. For example, subcircuit A can be the fused circuit shown in

Fig. S5b and subcircuit B can be the sparsified circuit shown in Fig. S5c. This analysis is similar to the behavior of the many replicas collapsing to a single qubit in the Suzuki-Trotter transformation, enabling a mapping between the thermodynamics of a many-body quantum system and a probabilistic system [72].

Going back to Eq. (S.4)-(S.5), and substituting  $m_A = m_B$  and calculating the input to the node  $m_A$  by  $I_A = -\partial E / \partial m_A$ :

$$I_A = \sum J_{Aj} m_j + \sum J'_{Bj} m_j \quad (\text{S.9})$$

Eq. S.9 shows the mathematical justification of adding the columns of fused nodes together, as shown in the composite circuit of Fig. S4. Note that the rows of fused nodes also need to be added together to ensure the symmetry of the J matrix.

## 2. Fused circuit

In a fused p-circuit, we combine the p-bits that represent the same signal to minimize the number of p-bits. For example, all the  $B_0$  signals get fused together in the 8-bit factorizer ( $m = 4$ ) p-circuit and we have only 1 p-bit instead of 4 p-bits for  $B_0$  (Supplementary Fig. S5a,b).

Thus, for the n-bit factorizer circuit in Fig. 1a, we have  $2m$  p-bits from the input bits of the AND gates. The output p-bits of the AND gates get fused with the corresponding input p-bits of the FAs, except the direct output of the first AND gate that represents  $S_0$ . It will be represented by a single p-bit. For the FAs, the first row has  $4m + 1$  p-bits instead of  $5m$ , since all the neighbor FAs have the  $c_{\text{out}}$  and  $c_{\text{in}}$  fused together. For the other rows of the FAs, we have  $3m + 1$  p-bits per row. This is because one of the input bits comes from the previous row. The number of p-bits in a fused n-bit factorizer p-circuit can be generalized as,

$$\begin{aligned} N_{\text{fact}} (\text{fused}) &= 2m + (4m + 1) + (3m + 1)(m - 2) + 1 \\ &= 3m^2 + m \end{aligned} \quad (\text{S.10})$$

where,  $m = \frac{n}{2}$ .

Likewise, the invertible logic SAT solver circuit in Fig. 1b can be composed using fusion. Supplementary Fig. S5d,e sketches a 4-clauses 3SAT solver p-circuit where the input variable 'q' is common to all the clauses. After fusion, it is represented by a single p-bit instead of 4 p-bits. This way, we have exactly one p-bit for each input variable. The output p-bits of the OR gates in the first row get fused with the corresponding input p-bits of the OR gates in the second row. To encode this, we need exactly one p-bit for each clause. Finally, all the output p-bits of the OR gates in the second row are fused together and represented by a single p-bit clamped to 1. The number of p-bits in a fused 3SAT p-circuit can be generalized as,

$$N_{\text{3SAT}} (\text{fused}) = c + v + 1 \quad (\text{S.11})$$

where,  $c$  = number of clauses, and  $v$  = number of input variables.

The fused p-circuit is software-friendly since it keeps the state space smaller, however, it introduces a fan-out issue in the sIM due to having too many neighbors for some p-bits. It also slows down the clock speed as discussed in the previous section.

## 3. Sparsified circuit

In a sparsified p-circuit, we do not fuse the p-bits when it exceeds a predefined maximum number of neighbors for any p-bit. Here, we demonstrate two different ways of sparsifying a graph, one with an example of the integer factorization and the other with an example of the 3SAT solver.

In the factorizer p-circuit, we add a series of p-bits to the same-signal input bits using copy gates. Having set a maximum number of neighbors,  $k$  for each p-bit, we add a p-bit for every  $(k - 1)$  input bits to be connected. If the total number of p-bits added is more than 1, the process is started again until only one p-bit is added, which represents the actual input p-bit. For example, let us consider  $B_0$  in the 8-bit factorizer p-circuit ( $m = 4$ ) in Supplementary Fig. S5c where we set  $k = 3$ . Thus, we add  $k - 1 = 2$  p-bits and connect them to a final p-bit representing  $B_0$ .

If no p-bits are fused, the n-bit factorizer circuit in Fig. 1a has  $3m^2$  p-bits for the  $m^2$  AND gates and  $5m(m - 1)$  p-bits for the  $m(m - 1)$  FAs. The number of p-bits for a sparsified n-bit factorizer p-circuit with a maximum number of neighbors,  $k$  per p-bit includes additional p-bits for the copy gates and can be generalized as,

$$\begin{aligned} N_{\text{fact}} (\text{sparse}) &= 3m^2 + 5m(m - 1) + 2mf(m, k) \\ &= 8m^2 - 5m + 2mf(m, k) \end{aligned} \quad (\text{S.12})$$

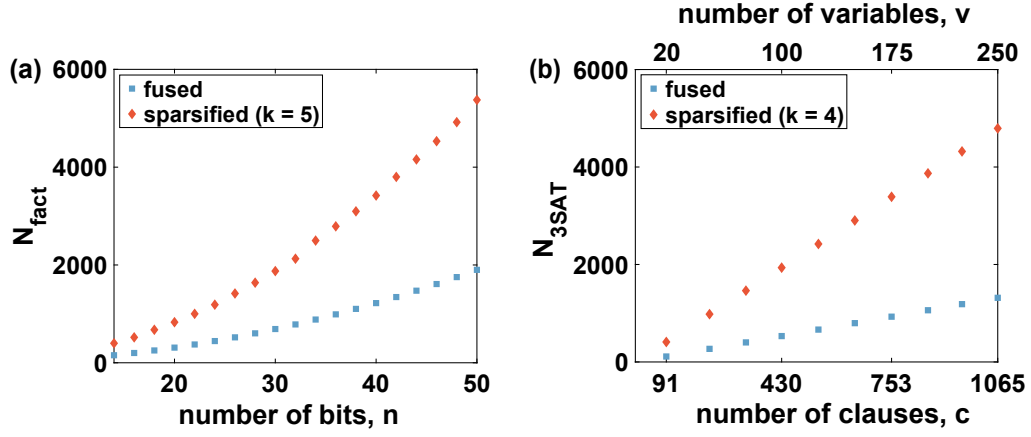


**FIG. S6.** Number of p-bits. (a)  $N_{\text{fact}}$  for the fused vs the sparsified factorizer p-circuit. (b)  $N_{\text{3SAT}}$  for the fused vs the sparsified 3SAT solver p-circuit.

where,

$$m = \frac{n}{2}$$

$$f(m, k) = \sum_{i=1}^{\lceil \log_{k-1} m \rceil} a_i$$

$$a_0 = m$$

$$a_i = \left\lceil \frac{a_{i-1}}{k-1} \right\rceil$$

In this work, we set  $k = 5$  for integer factorization and the expression can be approximated as,

$$N_{\text{fact}} (\text{sparse}) \approx 8m^2 - 5m + 2m \left\lceil \frac{m-1}{3} \right\rceil$$

$$\approx 8m^2 - 5m + 2m \frac{m-1}{3}$$

$$= 8m^2 - 5m + \frac{2}{3}m^2 - \frac{2}{3}m$$

$$= \frac{26}{3}m^2 - \frac{17}{3}m$$
(S.13)

For the 3SAT problem, instead of fusing, we connect the same-signal input bits by inserting a copy gate between every two input p-bits as shown in the 4-clauses 3SAT p-circuit in Supplementary Fig. S5f. This way, the input p-bits get correlated and also avoid additional neighbors. The output p-bits of the OR gates in the first row get fused with the corresponding input p-bits of the OR gates in the second row as before since it does not cost any fan-out issue. Finally, the output p-bits of the OR gates in the second row are fused in pairs and clamped to 1. Each clause has 2 OR gates and thus 5 p-bits since the middle p-bits get fused. However, since the output p-bits also get fused in pairs, we have 1 p-bit less for every 2 clauses. The final sparsified 3SAT solver p-circuit has a maximum number of neighbors  $k = 4$  only and the number of p-bits can be generalized as ( $c$ =number of clauses),

$$N_{\text{3SAT}} (\text{sparse}) = \lceil 5c - \frac{1}{2}c \rceil = \lceil \frac{9}{2}c \rceil$$
(S.14)

The sparsified p-circuit is hardware-friendly since it does not introduce any fan-out issue and allows fast clocks with small adder delay in the sIM as discussed in the previous section.

Fig. S6 reports the number of p-bits,  $N_{\text{fact}}$  and  $N_{\text{3SAT}}$  for both the fused and the sparsified versions of the factorizer and the 3SAT solver p-circuits respectively.

### K. Time to solution for exact factorization

We have reported exact factorization up to 32-bit semi-prime numbers in Section VI. Here, we report the time to find the exact factors. An exponential fit up with respect to the number of p-bits up to 5375 p-bits shows the difficulty in factoring numbers

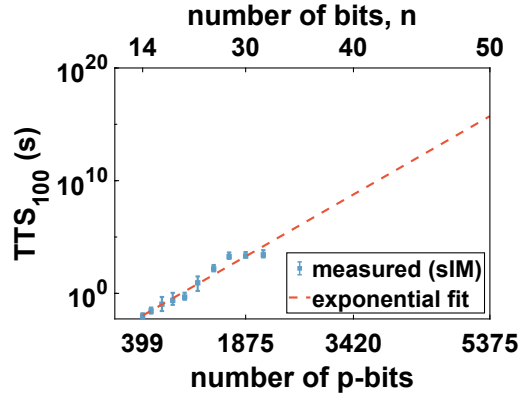


**FIG. S7.** Time to solution for exact factorization ( $TTS_{100}$ ) of 14-bit to 32-bit semi-prime numbers in the sIM and an exponential fit up with respect to the number of p-bits up to 5375 p-bits. The error bars are obtained by reporting  $TTS_{100}$  to factor 10 different numbers 10 times for each problem showing the maximum-minimum fluctuations.

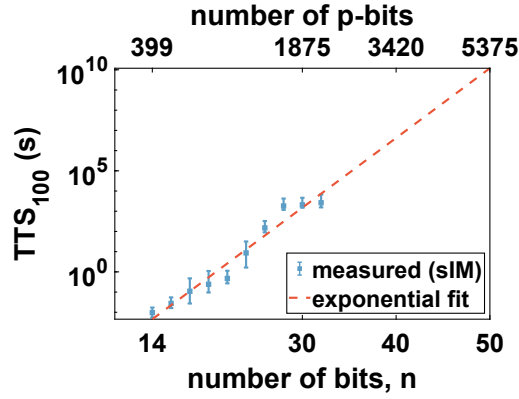


**FIG. S8.** Time to solution for exact factorization ( $TTS_{100}$ ) of 14-bit to 32-bit semi-prime numbers in the sIM and an exponential fit with respect to the number of bits up to 50-bits. The error bars are obtained by reporting  $TTS_{100}$  to factor 10 different numbers 10 times for each problem showing the maximum-minimum fluctuations.

larger than 32-bit with the current annealing schedule (Fig. S7). We have factored 10 different numbers 10 times for each problem to obtain the error bars showing the maximum and the minimum fluctuations. We describe this plot with the following equation:

$$t = t_0 \exp\left(-\frac{N}{\tau}\right) \quad (\text{S.15})$$

where  $N$  = number of p-bits,  $t = TTS$ ,  $t_0$  = pre-exponential factor,  $\tau$  = time constant. From the fitted plot, we obtain  $t_0 = 10^{-3.39}s$  and  $\tau = 122.13$ .

Another exponential fit up with respect to the number of bits up to 50-bits is shown in Supplementary Fig. S8. We describe this plot with the following equation:

$$t = t_0 \exp\left(-\frac{n}{\tau}\right) \quad (\text{S.16})$$

where  $n$  = number of bits. From the fitted plot, we obtain  $t_0 = 10^{-7.17}s$  and  $\tau = 1.26$ .